IEEE Access
Multidisciplinary | Rapid Review | Open Access Journal

Received October 24, 2019, accepted November 9, 2019, date of publication November 14, 2019,
date of current version November 25, 2019.

Digital Object Identifier 10.1109/ACCESS.2019.2953510

DBO Trajectory Planning and *HAHP* Decision-Making for Autonomous Vehicle Driving on Urban Environment

DEQUAN ZENG[1,2], ZHUOPING YU[1,2], LU XIONG[1,2], ZHIQIANG FU[1,2], PEIZHI ZHANG[1,2], AND HONGTU ZHOU[3]

[1]School of Automotive Studies, Tongji University, Shanghai 201804, China
[2]Clean Energy Automotive Engineering Centre, Tongji University, Shanghai 201804, China
[3]College of Electronics and Information Engineering, Tongji University, Shanghai 201800, China

Corresponding author: Lu Xiong (xiong_lu@tongji.edu.cn)

This work was supported in part by the National Key Research and Development Program of China under Grant 2018YFB0105103 and Grant 2018YFB0105101, and in part by the Science and Technology Commission of Shanghai under Grant 17DZ1100202 and Grant 16DZ1100701.

ABSTRACT A novel *driving behaviour oriented* (*DBO*) *trajectory planner* and *hierarchical analytic hierarchy process* (*HAHP*) *decision maker* are presented for intelligent vehicle. Since driving on structural road should satisfy actuator constraints and improve comfortableness as soon as possible, which strictly obeys traffic rules other than making traffic mess, it is rather than purely pursuing the shortest route/time. By analysis traffic rules, the*DBO* framework is employed to produce trajectories. To make trajectory drivable, cubic B-spline and clothoid curve are modeled to keep continuous curvature, and cubic polynomial curve is to schedule velocity profile satisfying stability and comfort. To pick out the best trajectory, *HAHP decision maker* is developed to evaluate the candidates. The first layer selects optimal paths considering smoothness and economy, and the second layer selects best trajectory taking smoothness, comfortableness and economy in account. Moreover, *DBO rapidly exploring random tree* (*RRT*) *replanner* is embedded to ensure algorithm completeness. Finally, several typical scenarios are designed to verify the real-time and reliability of the algorithm. The results illustrate that the algorithm has highly real-time and stability evaluated by *Statistical Process Control method* as the probability for the peak time less than 0.1s is 100% except three obstacles avoidance scenario is 59.31% in 1000 cycles. Since the planned trajectory is smooth enough and satisfy the constraints of the actuator, the mean lateral tracking error is less than 0.2m with 0.5m peak error, and the mean speed error less than 0.5km/h with 1.5km/h peak error for all scenarios.

INDEX TERMS Autonomous vehicle, trajectory planner, decision maker, urban environment, driving behavior orient, hierarchical analytic hierarchy process, statistical process control.

NOMENCLATURE

DBO	driving behaviour oriented
AHP	analytic hierarchy process
HAHP	hierarchical analytic hierarchy process
RRT	rapidly exploring random tree
k_{max}	maximum curvature of path
L_b	length of cubic B-spline control segment
α_b	included angle of cubic B-spline control segments
X_{c0}	the first node for lane change segment
X_{c1}	the second node for lane change segment
X_{c2}	the third node for lane change segment
X_{c3}	the fourth node for lane change segment
l_{c1}	length of $X_{c0}X_{c1}$
l_{c2}	length of $X_{c1}X_{c2}$
l_{c3}	length of $X_{c2}X_{c3}$
α_c	included angle between $X_{c0}X_{c1}$ and $X_{c1}X_{c2}$
θ_c	included angle between X_2X_3 and ox axis
X_{t0}	the first node for turn segment
X_{t1}	the second node for turn segment
X_{t2}	the third node for turn segment
X_{t3}	the fourth node for turn segment
X_{t4}	the fifth node for turn segment

The associate editor coordinating the review of this manuscript and approving it for publication was Xiaodong Sun.

X_{t5}	the sixth node for turn segment
s_{t1}	length of $X_{t0}X_{t1}$
s_{t2}	length of $X_{t1}X_{t2}$
s_{t3}	length of $X_{t2}X_{t3}$
s_{t4}	length of $X_{t3}X_{t4}$
s_{t5}	length of $X_{t4}X_{t5}$
a_{t1}	quadratic coefficient for clothoid of $X_{t1}X_{t2}$
b_{t1}	primary coefficient for clothoid of $X_{t1}X_{t2}$
c_{t1}	constant coefficient for clothoid of $X_{t1}X_{t2}$
a_{t2}	quadratic coefficient for clothoid of $X_{t3}X_{t4}$
b_{t2}	primary coefficient for clothoid of $X_{t3}X_{t4}$
c_{t2}	constant coefficient for clothoid of $X_{t3}X_{t4}$
θ_{t1}	heading of X_2 node
θ_{t2}	heading of X_3 node
θ_{t3}	heading of X_4 node
R_t	radius for arc of $X_{t2}X_{t3}$
G	target point
$\{g_i\}_{i=0,\ldots,m}$	target set sampled along the lateral of G
m	number of sampled target points
d_G	lateral offset of G
l	length of vehicle
w	width of vehicle
d	distance of two circle center for collision check
r	circle radius for collision check
S_x	x pose for Gaussian sampling node
S_y	y pose for Gaussian sampling node
x_{c0}	x pose of reference node for Gaussian sampling
y_{c0}	y pose of reference node for Gaussian sampling
r_s	Gaussian sampling radius
θ_s	Gaussian sampling angle
r_{s0}	Gaussian sampling radius offset
θ_{s0}	Gaussian sampling angle offset
σ_r	Gaussian radius standard deviation
σ_θ	Gaussian angle standard deviation
r_{rand}	Gaussian sampling random radius
θ_{rand}	Gaussian sampling random angle
v_{car0}	vehicle start speed
a_{car0}	vehicle start acceleration
v_{carg}	vehicle target speed
a_{carg}	vehicle target acceleration
S_g	path length
v_{max}	maximum vehicle speed
v_{car}	vehicle speed
a_{acc}	vehicle acceleration
a_{max}	vehicle maximum acceleration
a_{min}	vehicle minimum acceleration
a_y	vehicle lateral acceleration
a_{ymax}	vehicle maximum lateral acceleration
v_{ay}	vehicle speed limited by maximum lateral acceleration
k_{node}	node curvature
μ	road adhesion coefficient
g	gravitational acceleration
v_{allow}	allowed speed
Δv	safety margin of vehicle speed
κ_B	maximum curvature of path
κ_C	minimum curvature of path
κ_g	sum of squared curvature
$d\kappa_g$	sum of squared deviation of curvature
l_{off}	lateral offset from reference path
a_g	sum of squared longitude acceleration
da_g	sum of squared derivation of longitude acceleration
t_g	total of time consumption for trajectory execution
N	number of nodes for path
s_i	distance from path node i to node i+1
a_i	acceleration of path node i
k_i	curvature of path node i
n	offset interval of target point
t_i	time consumption from path node i to node i+1
RI	random index of Saaty's fundamental scale
nc	criteria in the same level comparison value
CR	consistency ratio for judgment matrix
CI	consistency index
λ	eigenvalue
λ_{max}	the maximum eigenvalue
W	normalized eigenvectors
w_a	eigenvectors
A_{static}	factor of optimal paths
$B_{1static}$	factor of path smoothness
$B_{2static}$	factor of path economy
$C_{1static}$	factor of path length
$C_{2static}$	factor of sum of squared path curvature
$C_{3static}$	factor of sum of squared deviation of path curvature
$C_{4static}$	factor of lateral offset of path
$A_{dynamic}$	factor of optimal trajectory
$B_{1dynamic}$	factor of trajectory smoothness
$B_{2dynamic}$	factor of trajectory comfortableness
$B_{3dynamic}$	factor of trajectory economy
$C_{1dynamic}$	factor of trajectory length
$C_{2dynamic}$	factor of sum of squared trajectory curvature
$C_{3dynamic}$	factor of sum of squared deviation of trajectory curvature
$C_{4dynamic}$	factor of lateral offset of trajectory
$C_{5dynamic}$	factor of sum of squared longitude acceleration

$C_{6dynamic}$	factor of sum of squared derivation of longitude acceleration
$C_{7dynamic}$	factor of peak lateral acceleration
$C_{8dynamic}$	factor of total of time consumption
ω_j	comprehensive weight of index j
b_i	weight of index i
RI_i	random index of index i
CI_i	consistency index of index i
μ_t	mean time for *DBO* and *HAHP* process
σ_t	mean square error for *DBO* and *HAHP* process
t_{max}	maximum time for *DBO* and *HAHP* process
$P(t \leq 0.1\text{s})$	the probability for t_{max} less than 0.1s

I. INTRODUCTION

Lots of attentions have been payed to trajectory planning and decision making as two key parts of the core technology for autonomous vehicle [1], [2], which is white hope for alleviating the increasingly severe traffic pressure, significantly improving road traffic safety and reducing emissions [3], [4] in recently.

As a classical implementation, *Dijkstra* [5] algorithm, based on breadth first search strategy, searches for best trajectory by sorting length. In order to speed up algorithm, A^* [6] introduces the heuristic value, which estimates the cost from the current node to target node, into *Dijkstra* cost function. And *anytime weight* A^* [7] set weight factor ε ($\geq$ 1) to increase the proportion of heuristic value in the evaluation function, forcing the search of nodes to be more inclined to the target node. Different from *anytime weight* A^* with fixed weight factor, *anytime repairing* A^* [8] dynamically adjusts the factor to search for the better path. Since environmental information is not exactly known, D^* algorithm will make use of the unaffected node information to replan [9]. Due to the constraints of vehicle steering mechanism, the results of the above algorithm are not suitable for direct execution. Therefore, *hybrid* A^* [10] and *state lattic*e [11], which the former is derived by improving node extension and the latter derived by improving node connection, are the latest development directions of search algorithms. However, as the configuration is the discrete grid, the results based on the search method need further smoothing before the vehicle could track [12]. Differ from search methods, *RRT* (*Rapidly-Exploring Random Tree*) [13] represents the sampling-based method [14] that is extended to obtain nodes in continuous feature space. In order to improve the real-time performance, *Bi-RRT* (*Bidirectional RRT*) is derived as bidirectional expansion from the start node and target node [15] and *H-RRT* (*Heuristic RRT*) employs heuristic function to extend low cost nodes [16]. However, the sample-based algorithm always contains a random seed generator, so it inevitably contains zigzags [12] leading to the planning results should be postprocessed for smoothing [17].

For generating path making vehicle directly track possible, unremitting efforts have been made to the implementation of *B-spline* [18], *Bezier-spline* [19], *clothoid* [20], *polynomial curve* [21] and *model predictive control* (*MPC*) *planner* [22], which could realize curvature continuity. However, since the above methods are incompleteness [4], it is necessary to generate lots of trajectories covering the configuration as far as possible by sampling target set [23]. At the same time, the optimal trajectory execution is picked out by combining the requirements of multiple objectives, such as safety [24], comfort [25], economy [26], etc. Literature [27] constructs a linear optimal objective function by taking the offset from path to road boundary, the path curvature and the path length as indicators. Similarly, literature [28] constructs a linear preferential function with the indexes of total time, acceleration squared, acceleration increment squared, illegal velocity and collision safety. Furthermore, literature [29] constructs linear objective functions from static and dynamic aspects respectively. However, the linear objective function constructed by the existing single weighting method has a large deviation, and the index calculation covers the subjective and objective parts, which is easy to generate weight preference and poor robustness. Therefore, *analytic hierarchy process* (*AHP*) is introduced to realize the quantitative expression of subjective and objective indexes [30], since *AHP* is a multiple criteria decision-making tool, which could be employed to measure the relative dominance or preference of elements related to a main objective [31]. As the main advantage of *AHP* is that the importance of each element is determined by using paired comparisons generating better results [32], it is widely used in decision making for *UAV* optimal trajectory [33]–[35] and site rational planning [36]–[38].

Aimed at improving performance of intelligent vehicle driving on urban environment, *DBO trajectory planner* and *HAHP decision maker* are proposed in this paper. Considering the vehicle's non-holonomic constraints and the particularity of structural road, *DBO trajectory planner*, which is embedded *DBO RRT path replanner* to ensure algorithm completeness, generates human-like trajectory set with curvature continuous. And *HAHP* decision maker is prudentially developed to pick out the best trajectory since taking smoothness, comfortableness and economy into account. As shown in Figure 1, *DBO path planner* mainly takes lane change, turn left and turn right into account, according to the rules and the daily behavior of drivers. After *collision checking*, the safety paths are packed as candidates delivering to *HAHP decision making*. If there are no viable safety path, the *DBO RRT path planner* is triggered, as much as possible, to find a viable trajectory of existence. After candidate path generated, cubic polynomial curve is employed to schedule velocity profile for meeting the vehicle stability requirements, actuator constraints and comfort conditions. Finally, to pick out the best trajectory produced by *DBO trajectory planner*, *hierarchical analytic hierarchy process* (*HAHP*) *decision maker* is prudentially developed to evaluate the candidates. The first layer is *path decision maker*, which selects optimal paths considering smoothness and economy by taking four static indexes in account. And *trajectory decision maker*, as the second

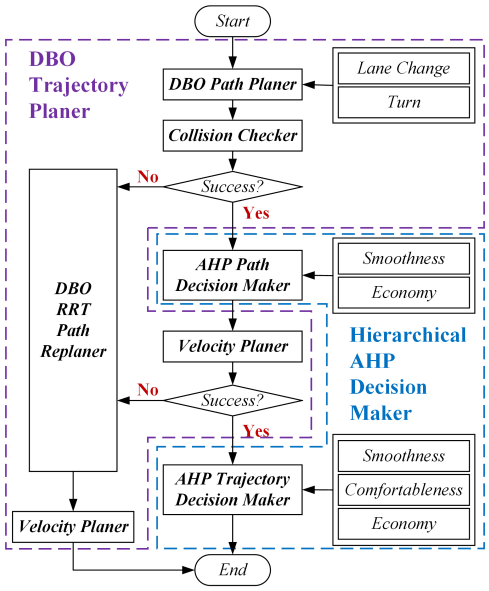

FIGURE 1. Strategy framework.

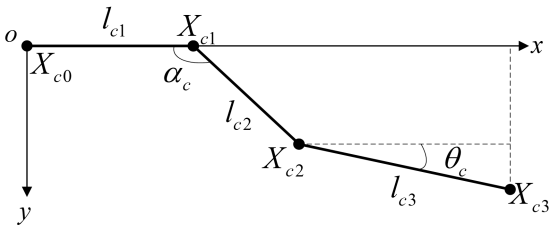

FIGURE 2. Lane changing control segments.

layer, selects best trajectory considering smoothness, comfortableness and economy by taking eight dynamic indexes in account. The rest of this paper is organized as follows. In the second section, each part of *DBO Trajectory Planer* is discussed in detail. In the third section, it is detailed formulation of *HAHP Decision Maker*. In the fourth section, the experiments and results are discussed. In final section, it is conclusion.

II. DBO TRAJECTORY PLANER

A. DBO PATH PLANER

1) LANE CHANGING

The cubic B-spline curve is employed to generate lane changing path for curvature continuous. The maximum curvature of the path is [39]–[41],

$$k_{\max} \geq \frac{1}{6}\frac{\sin\alpha_b}{L_b}\left(\frac{1-\cos\alpha_b}{8}\right)^{-1.5} \tag{1}$$

where k_{max} is the maximum curvature of path generated by cubic B-spline curve, L_b is length of cubic B-spline control segment, and α_b is included angle between the control segments.

Under the premise of curvature continuity and maximum curvature controllable, the method of generating lane changing path with three control segments is simple in construction and low in computational complexity in practically. As shown in Fig.2, $X_{c0}X_{c1}$, $X_{c1}X_{c2}$ and $X_{c2}X_{c3}$ are the control segments. For given start point X_{c0} and target point X_{c3}, the lane changing path planning problem is,

$$\begin{cases} \min J_c = \sum_{i=1}^{3} l_{ci} \\ s.t.\ (x_{c0}, y_{c0}) = (X_{c0}.x, X_{c0}.y)\,, \\ (x_{c3}, y_{c3}) = (X_{c3}.x, X_{c3}.y)\,, \\ (x_{c1}, y_{c1}) = (x_{c0} + l_{c1}, y_0) \\ x_{c2} = x_{c1} - l_{c2}\cos\alpha_c = x_{c3} - l_{c3}\cos\theta_c, \\ y_{c2} = y_{c1} + l_{c2}\sin\alpha_c = y_{c3} - l_{c3}\sin\theta_c, \\ l_{ci} > 0, \\ k_{\max} \geq \frac{1}{6}\frac{\sin\alpha_c}{\min(l_{c1}, l_{c2})}\left(\frac{1-\cos\alpha_c}{8}\right)^{-1.5} \\ k_{\max} \geq \frac{1}{6}\frac{\sin(\alpha_c+\theta_c)}{\min(l_{c2}, l_{c3})}\left(\frac{1-\cos(\alpha_c+\theta_c)}{8}\right)^{-1.5} \end{cases} \tag{2}$$

where l_{c1}, l_{c2}, l_{c3} is the length of $X_{c0}X_{c1}, X_{c1}X_{c2}, X_{c2}X_{c3}$, α_c is included angle between $X_{c0}X_{c1}$ and $X_{c1}X_{c2}$, and θ_c is included angle between $X_{c2}X_{c3}$ and ox axis.

The generated lane changing path is shown in Fig.3(a) and the curvature in Fig.3(b) (the green spline). As the experimental vehicle with the maximum turning curvature 0.25/m (the red lines in Fig.3(b)), the result illustrated the generated path is smooth enough and continuous to vehicle track.

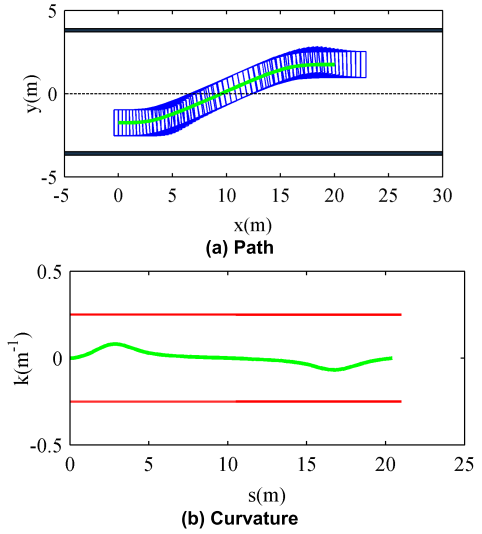

FIGURE 3. Lane changing path.

2) TURN

In practical, the turn paths should avoid crossing lanes when leaving and entering lanes for safety reasons. Considering the inevitable errors when vehicle tracks a path, as shown in Fig.4, two straight segments ($X_{t0}X_{t1}$ and $X_{t4}X_{t5}$) are added at the beginning and end of the path to reduce the lateral error of tracking for ensuring that the vehicle is always in a lane. Then, two clothoids ($X_{t1}X_{t2}$ and $X_{t3}X_{t4}$) are employed to smooth the path for curvature continuity. In addition, an arc

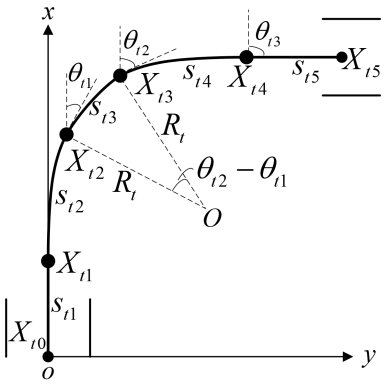

FIGURE 4. Turn control segments.

segment ($X_{t2}X_{t3}$) is constructed to reduces curvature jitter and space required for turning. For given start point X_{t0} and target point X_{t5}, the turning path planning problem is,

$$\begin{cases} \min J_t = \sum_{i=1}^{5} s_{ti} \\ s.t.\ (x_{t0}, y_{t0}) = (X_{t0}.x, X_{t0}.y)\,, \\ (x_{t5}, y_{t5}) = (X_{t5}.x, X_{t5}.y)\,, \\ s_{ti} > 0, \quad i = 1, \ldots, 5 \\ \dfrac{1}{R_t} = k_t \le k_{\max} \end{cases} \tag{3}$$

As shown in Fig.4, the supplementary constraints from start segments to target segments are as follows [40], [41]:

(1) the first segment is a straight line s_{t1},

$$\begin{cases} x_{t1} = x_{t0} + s_{t1} \\ y_{t1} = y_{t0} \end{cases} \tag{4}$$

where s_{t1} is the length of a straight line.

(2) the second segment is a clothoid s_{t2},

$$\begin{cases} a_{t1}s_{t2}^2 + b_{t1}s_{t2} = \dfrac{1}{R} \\ \dfrac{1}{3}a_{t1}s_{t2}^3 + \dfrac{1}{2}b_{t1}s_{t2}^2 = \theta_{t1} \\ x_{t1} + \int_0^{s_{t2}} \cos\left(\dfrac{1}{3}a_{t1}s^3 + \dfrac{1}{2}b_{t1}s^2\right) ds = x_{t2} \\ y_{t1} + \int_0^{s_{t2}} \sin\left(\dfrac{1}{3}a_{t1}s^3 + \dfrac{1}{2}b_{t1}s^2\right) ds = y_{t2} \end{cases} \tag{5}$$

where s_{t2} is the length of clothoid, a_{t1}, b_{t1}, c_{t1} is coefficient of clothoid, R_t is radius of arc and θ_{t1} is heading of X_{t2} node.

(3) the third segment is a arc s_{t3},

$$\begin{cases} x_{t2} = R_{tx} - R_t \sin\theta_{t1} \\ y_{t2} = R_{ty} + R_t \cos\theta_{t1} \\ x_{t3} = R_{tx} - R_t \sin\theta_{t2} \\ y_{t3} = R_{ty} + R_t \cos\theta_{t2} \\ s_{t3} = (\theta_{t2} - \theta_{t1}) \cdot R_t \end{cases} \tag{6}$$

where s_{t3} is the length of arc and θ_{t2} is heading of X_{t3} node.

(4) the fourth segment is a clothoid s_{t4},

$$\begin{cases} c_{t2} = \dfrac{1}{R} \\ a_{t2}s_{t4}^2 + b_{t2}s_{t4} + c_{t2} = 0 \\ \dfrac{1}{3}a_{t2}s_{t4}^3 + \dfrac{1}{2}b_{t2}s_{t4}^2 + c_{t2}s_{t4} + \theta_{t2} = \theta_{t3} \\ x_{t3} + \int_0^{s_{t4}} \cos\left(\dfrac{1}{3}a_{t2}s^3 + \dfrac{1}{2}b_{t2}s^2 + c_{t2}s + \theta_{t2}\right) ds = x_{t4} \\ y_{t3} + \int_0^{s_{t4}} \sin\left(\dfrac{1}{3}a_{t2}s^3 + \dfrac{1}{2}b_{t2}s^2 + c_{t2}s + \theta_{t2}\right) ds = y_{t4} \end{cases} \tag{7}$$

where s_{t4} is the length of clothoid, a_{t2}, b_{t2}, c_{t2} is coefficient of clothoid, R_t is radius of arc, θ_{t3} is heading of X_{t4} node.

(5) the fifth segment is a straight line s_{t5},

$$\begin{cases} x_{t5} = x_{t4} + s_{t5} \cdot \cos\theta_{t3} \\ y_{t5} = y_{t4} + s_{t5} \cdot \sin\theta_{t3} \end{cases} \tag{8}$$

where s_{t5} is the length of a straight line.

The generated turning path is shown in Fig.5(a) and the curvature, in Fig.5(b) (the green spline), is smooth enough and continuous with less continuous direction change which means tracking the path will make passengers comfortable as steering wheel's smooth change.

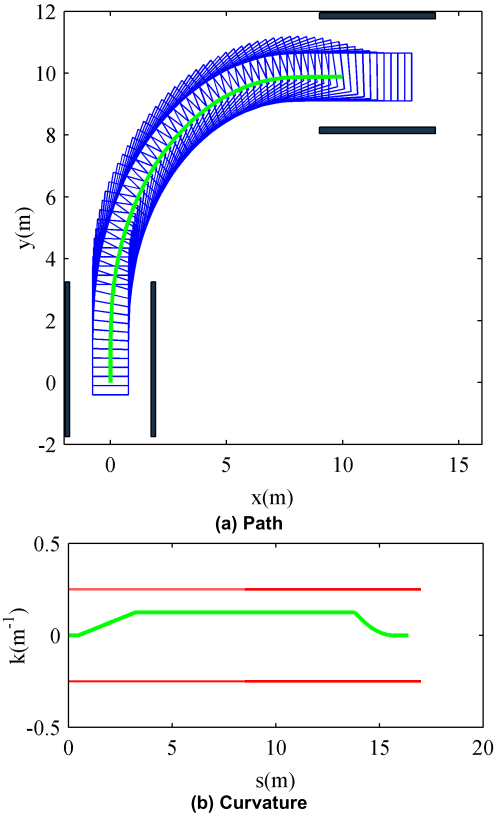

FIGURE 5. Turning path.

3) PATH SET

After the target point given by decision making, such as G point shown in Fig.6, the target set $\{g_i\}_{i=0,\ldots,m}$ sampled along

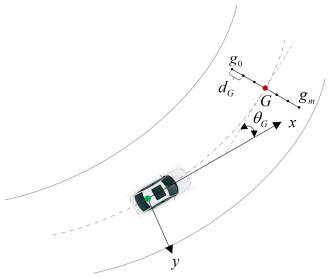

FIGURE 6. Target set sampling.

the lateral of target point with offset d_G, of which prevent vehicle from crossing solid lanes. All the sampling points have the same heading and curvature with target point.

In general, the sample for lane changing is limited in [−5.25m, 5.25m] due to the lane changing behavior is restricted to an adjacent lane and the standard urban road width is 3.5m. As shown in Fig.7(a), there are 31 lane changing paths and the path's curvature is satisfied the requirements of continuity and peak constraints as shown in Fig.7(b) (the rad lines are the peak constraints according to minimum turning radius of vehicle). Similarly, there are 322 turning paths as shown in Fig.8(a) and the path's curvature is satisfied the requirements of continuity and peak constraints as shown in Fig.8(b).

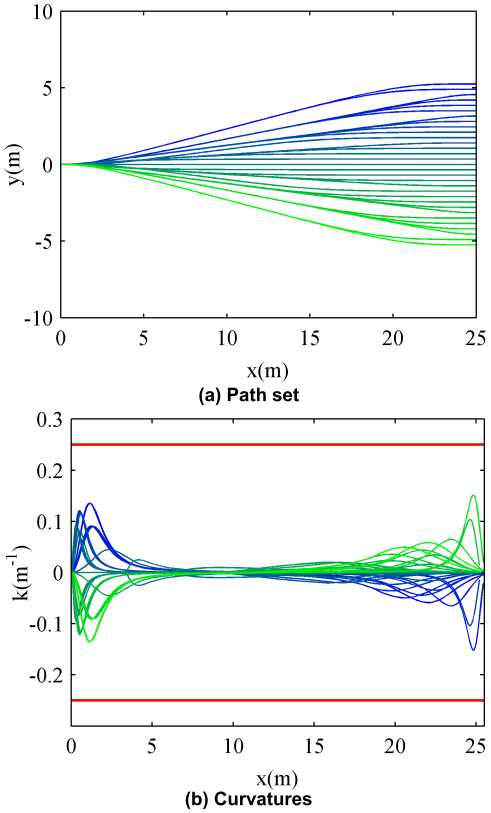

FIGURE 7. Lane changing path set.

B. COLLISION CHECKER

After generating paths, it is essential to check the collision of the set and picking out the safe ones as candidates for

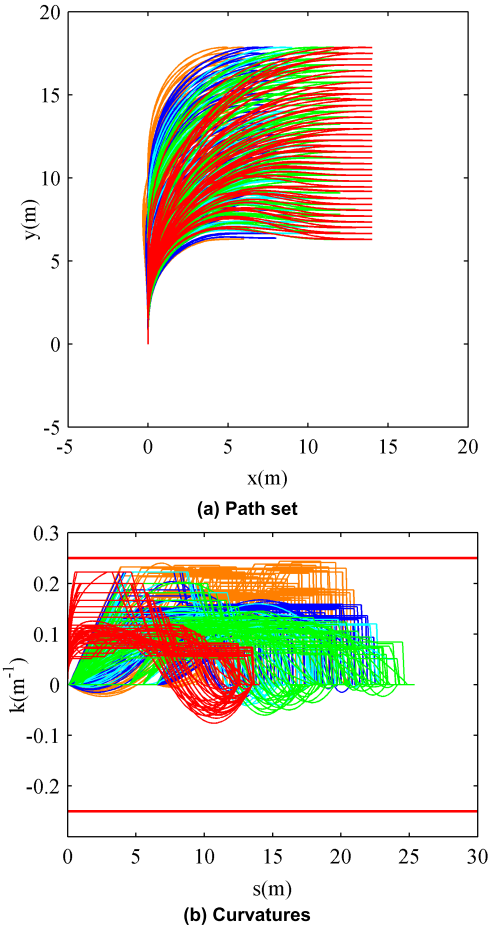

FIGURE 8. Turning path set.

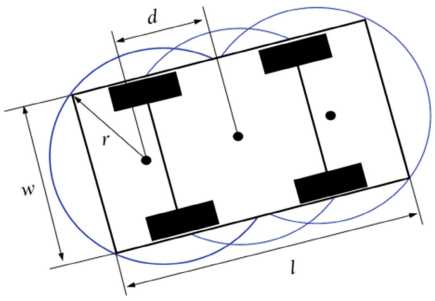

FIGURE 9. Vehicle configuration for collision checking.

planning velocity to form candidate trajectories. To achieve rapid collision detection, three circles with same radius r are employed to cover the vehicle, which are along the longitudinal direction as shown in Fig.9. The radius of circle is,

$$\left(\frac{l-2d}{2}\right)^2+\left(\frac{w}{2}\right)^2=r^2 \tag{9}$$

where l is length of vehicle, d is distance of two circle's center, r is circle's radius, w is width of vehicle.

As the environment around the smart vehicle being described by occupying a grid, in which static obstacles are

labeled as 1, dynamic obstacles as 2 and no obstacles as 0, the planned path set, the path is collision-free when the grids occupied by the circles of vehicle are all 0. As depicted in Fig.10, there are lots of grid in circles of vehicle are 1, which means the path is unsafe.

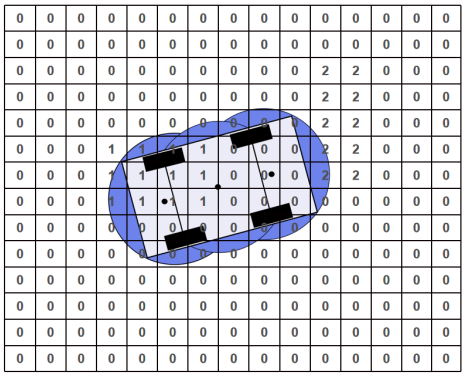

FIGURE 10. Collision checking in grid map.

C. DBO-RRT PATH REPLANNER

Due to *DBO* path planner is not completeness, an *DBO-RRT* path replanner is designed to find the existed path after all the path set generated by *DBO* path planer being checked as unsafe or, even, there is no path generated at all. Considering the search efficiency to reduce the time consumption of the algorithm, the *DBO-RRT* path replanner employs driver behavior as guide. As shown in Fig.11, the sampling node locates in the shaded area of a fan, which formed by Gaussian sampling distribution.

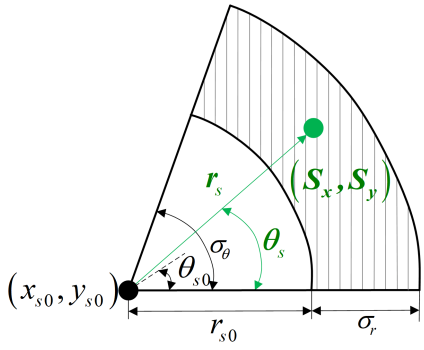

FIGURE 11. Gaussian sampling distribution.

The Gaussian sampling distribution satisfies that,

$$\begin{cases} S_x = x_{s0} + r_s \cos\theta_s \\ S_y = y_{s0} + r_s \sin\theta_s \end{cases} \tag{10}$$

where (S_x, S_y) is the sampled node, (x_{s0}, y_{s0}) is reference node and (r_s, θ_s) is Gaussian parameters, which is defined as follow,

$$\begin{cases} r_s = \sigma_r r_{rand} + r_{s0} \\ \theta_s = \sigma_\theta \theta_{rand} + \theta_{s0} \end{cases} \tag{11}$$

where (r_{s0}, θ_{s0}) is offset parameter and $(\sigma_r, \sigma_\theta)$ is Gaussian standard deviation, and $(r_{rand}, \theta_{rand})$ is random parameters.

Considering the driving behaviour, the Gaussian sampling zones are design as follows: 1) For lane changing behaviour, a fixed one is employed to Gaussian sampling. 2) For turning behaviour, two joint smaller fans are used for Gaussian sampling in first. If there are no effect node, an almost quadrant is applied.

For lane changing, as shown in Fig.12(a), a fixed fan is the Gaussian sampling area, with the start point $\boldsymbol{n_{init}}$ as center and the distance from start to goal point $\boldsymbol{n_{goal}}$ as radius. And Gaussian sampling nodes are the red circles shown in Fig.12(b). Similarly, there are two situations of the Gaussian sampling for turning: the first one is two joint smaller fans (as the fan $\boldsymbol{A}$ and fan $\boldsymbol{B}$ shown in Fig.13(a)), and the other is almost a quadrant (as fan $\boldsymbol{C}$ shown in Fig.13(a)). If the goal point is not extended within the two joint fans, switch to sample fan $\boldsymbol{C}$. The sampling nodes are shown in Fig.13(b).

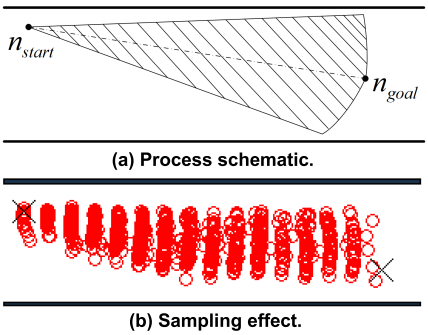

FIGURE 12. Gaussian sampling for lane changing.

Fig.14(a) shows a scenario that lane changing path generated by *DBO-RRT* path replanner as two obstacles too close to produce path by *DBO* path planer. As illustrated in Fig.14(b), the generated path has continuous smooth curvature (the green curve) and meets the constraints of peak curvature (the red lines).

Similarly, Fig.15(a) shows a scenario that turning path generated by *DBO-RRT* path replanner as a circular barrier formed by accidents at intersections too close to generate path by *DBO* path planer. As illustrated in Fig.15(b), the generated path has continuous smooth curvature (the green curve) and meets the constraints of peak curvature (the red lines).

D. VELOCITY PLANER

As candidate paths picking out, the velocity planner schedule speed profile for combining paths to form candidate trajectories, which should take some boundary conditions and dynamic constraints into account. In general, the boundary conditions are start speed and acceleration (v_{car0}, a_{car0}), target speed and acceleration (v_{carg}, a_{carg}) and path length S_g. To satisfy the requirements of actuator stability and passenger comfort, the dynamic constraints mainly are maximum longitudinal speed v_{max}, maximum and minimum lateral acceleration (a_{min}, a_{max}) and maximum lateral acceleration a_{ymax}

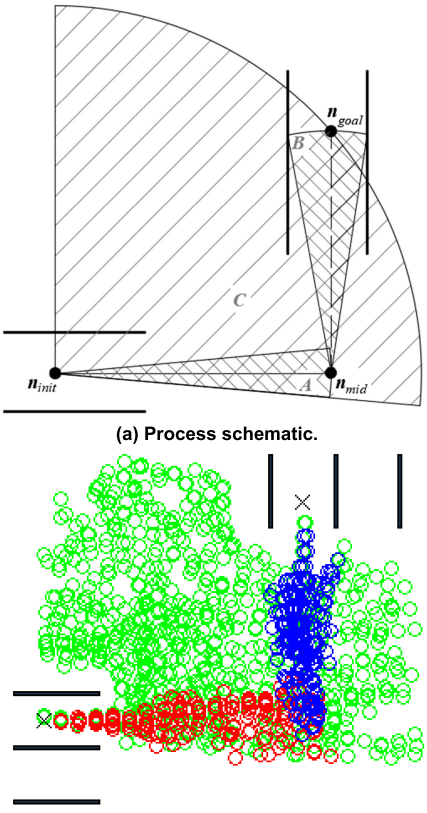

(a) Process schematic.

(b) Sampling effect.

FIGURE 13. Gaussian sampling for turning.

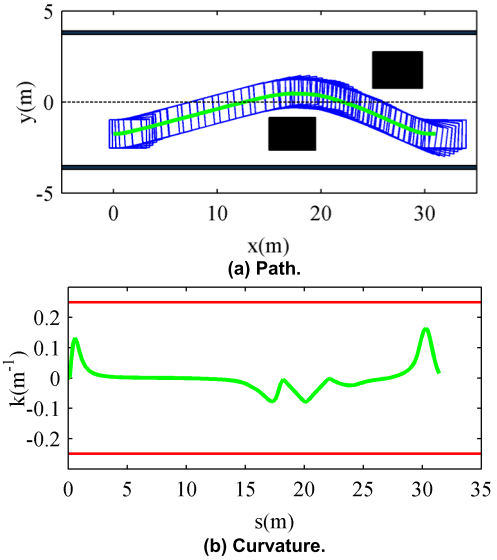

(a) Path.

(b) Curvature.

FIGURE 14. Lane changing path generated by ***DBO-RRT*** path replanner.

as defined as follows,

$$\begin{cases} v_{car} \le v_{\max} \\ a_{\min} \le \dot{v}_{car} = a_{acc} \le a_{\max} \\ |a_y| = v_{ay}^2 \, |k_{node}| \le a_{y\max} = 0.4\mu g \end{cases} \tag{12}$$

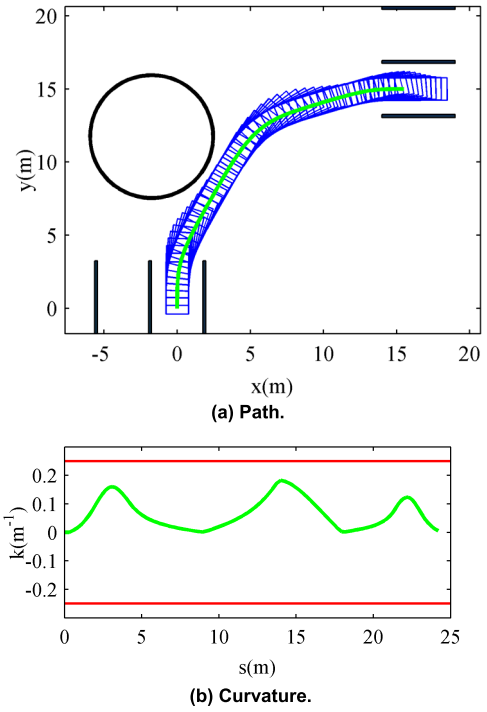

(a) Path.

(b) Curvature.

FIGURE 15. Turning path generated by ***DBO-RRT*** path replanner.

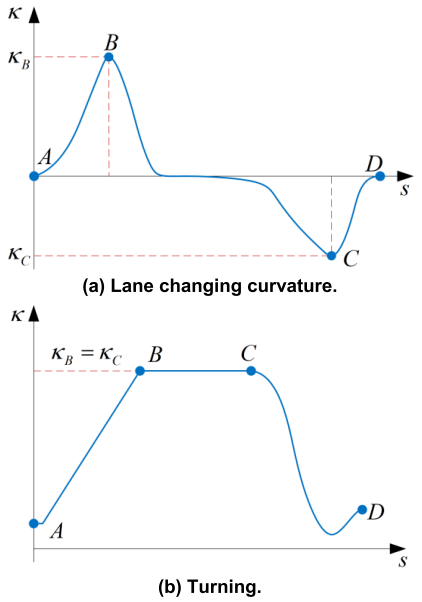

(a) Lane changing curvature.

(b) Turning.

FIGURE 16. Curvature profile of a typical path.

where v_{car} is vehicle speed, a_{acc} is vehicle acceleration, a_y is lateral acceleration, v_{ay} is vehicle speed limited by maximum lateral acceleration, k_{node} is curvature of node, μ is road adhesion coefficient, g is gravitational acceleration.

Taking the uncertainty of actuators into account, a certain safety margin Δv is involved in the speed allowed v_{allow} as,

$$v_{allow} = \min\left\{v_{\max}, v_{ay}\right\} - \Delta v \tag{13}$$

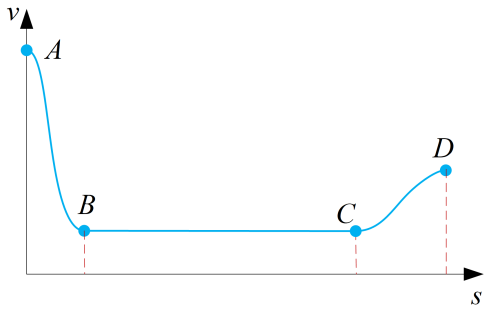

FIGURE 17. Velocity profile.

Due to the curvature of path being a critic constraint for velocity planning, it is necessary and convenient to use extreme curvature to guide speed planning. As shown in Fig.16, both typical lane changing and turning path have same trend of maximum and minimum curvature (κ_B and κ_C). For reducing time consumption and improving comfort, it is fruitful to keep the vehicle running at a constant speed as far as possible. Finally, the velocity profile consists of three segments, as depicted in Fig.17, that start segment (***AB*** curve) takes path's maximum curvature and initial speed into account, constant segment (***BC*** line) keeps constant allowable velocity and terminal segment (***CD*** curve) adjusts velocity according to target speed.

III. HAHP DECISION MAKER

A. EVALUATION INDEXES

TABLE 1. Compute formulas for evaluation indexes.

Index	Formula	Index	Formula
S_g	$\sum_{i=1}^{N-1} s_i$	a_g	$\sum_{i=1}^{N} a_i^2$
κ_g	$\sum_{i=1}^{N} \kappa_i^2$	da_g	$\sum_{i=2}^{N} \left(\frac{a_i - a_{i-1}}{t_i - t_{i-1}} \right)^2$
$d\kappa_g$	$\sum_{i=2}^{N} \left(\frac{\kappa_i - \kappa_{i-1}}{s_i - s_{i-1}} \right)^2$	a_{ymax}	$a_{y\max}$
l_{off}	$n \cdot d_G$	t_g	$\sum_{i=1}^{N-1} t_i$

where N is number of nodes for path, s_i is distance from path node i to node $i+1$, a_i is acceleration for path node i, κ_i is curvature for path node i, n is offset interval for target point, t_i is time consumption from path node i to node $i+1$.

Since the path expresses the state change in space without state in time, the indexes extracted from the path performance are only four static criteria listed below:

(1) Path length S_g;
(2) Sum of curvature squared κ_g;
(3) Sum of squared derivation of curvature $d\kappa_g$;
(4) Lateral offset from reference path l_{off}.

For a complete trajectory, which contains spatial-temporal state changes, the indexes extracted are four more dynamic criteria as follows:

(5) Sum of longitude acceleration squared a_g;

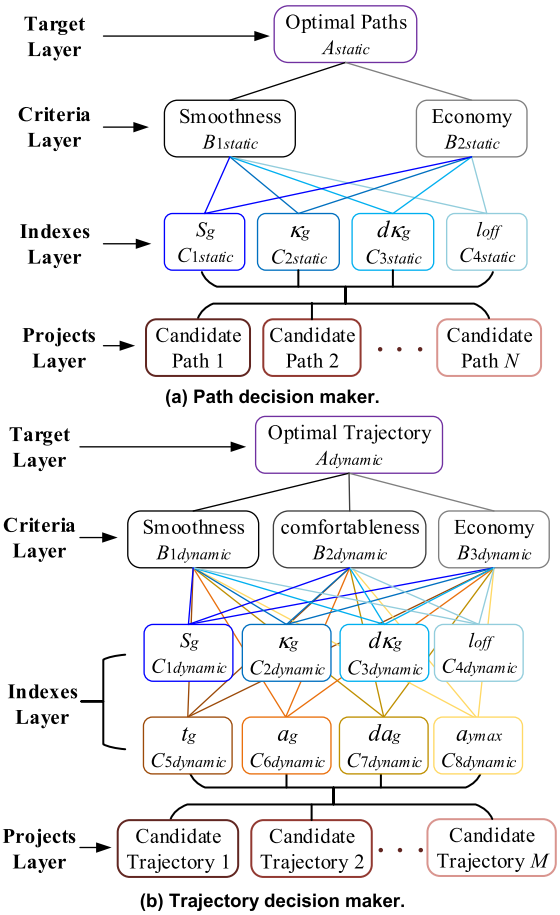

FIGURE 18. Hierarchical AHP decision maker.

(6) Sum of squared derivation of longitude acceleration da_g;
(7) Peak lateral acceleration a_{ymax};
(8) Total of time consumed for trajectory execution t_g.

All the compute formulas for evaluation criteria are listed in Table 1.

B. HIERARCHICAL AHP MODEL

1) MODEL DESIGN

Although collision detection removes some unsafe paths, the rest paths are still substantial as path DBO path planning generating lots of path. It is extremely time consuming and pointless to make decision for best trajectory from all candidate trajectories, which generated by planning velocity profiles for all rest paths. Therefore, a hierarchical AHP model for decision making is designed as shown in Figure.18. In the first step is path decision maker, which selects optimal paths in moderation from lots of candidate paths generated by DBO path planer, considering the criterion of smoothness and economy by taking the static indexes in account, mainly including path length S_g, sum of curvature squared κ_g, sum of squared derivation of curvature $d\kappa_g$ and lateral offset from reference path l_{off}. After processing by velocity planer, the selected optimal paths combining with velocity profiles form candidate trajectories. Since candidate trajectories are

generated by scheduling velocity for path, there are four new dynamic indicators employed to the trajectory decision maker, compared with path decision maker with only four static indicators. Therefore, the smoothness and economy should be recalculated as more indicators involved. Finally, trajectory decision maker selects optimal trajectory from lots of candidate trajectories, considering the criterion of smoothness, comfortableness and economy by taking the dynamic indexes in account, mainly including path length S_g, sum of curvature squared κ_g, sum of squared derivation of curvature $d\kappa_g$, lateral offset from reference path l_{off}, sum of longitude acceleration squared a_g, sum of squared derivation of longitude acceleration da_g, peak lateral acceleration a_{ymax} and total of time consumed for trajectory execution t_g. Where A_{static} is factor of optimal paths, $B_{1static}$ is factor of path smoothness, $B_{2static}$ is factor of path economy, $C_{1static}$ is factor of path length, $C_{2static}$ is factor of sum of squared path curvature, $C_{3static}$ is factor of sum of squared deviation of path curvature, $C_{4static}$ is factor of lateral offset of path, $A_{dynamic}$ is factor of optimal trajectory, $B_{1dynamic}$ is factor of trajectory smoothness, $B_{2dynamic}$ is factor of trajectory comfortableness, $B_{3dynamic}$ is factor of trajectory economy, $C_{1dynamic}$ is factor of trajectory length, $C_{2dynamic}$ is factor of sum of squared trajectory curvature, $C_{3dynamic}$ is factor of sum of squared deviation of trajectory curvature, $C_{4dynamic}$ is factor of lateral offset of trajectory, $C_{5dynamic}$ is factor of sum of squared longitude acceleration, $C_{6dynamic}$ is factor of sum of squared derivation of longitude acceleration, $C_{7dynamic}$ is factor of peak lateral acceleration, $C_{8dynamic}$ is factor of total of time consumption.

2) JUDGMENTS MATRIX AND CONSISTENCY CHECK

For each level, a pairwise comparison matrix is obtained based on the decision maker's judgments. As listed in Table 2, B_1,.., B_N is current layer factors, N is number of criterion of current layer, A_i is factor of criterion for the previous layer, b_{jk} is the Saaty's fundamental scale of B_j over B_k to A_i. The nc criteria in the same level are compared using Saaty's 1-to-9 scale as listed in Table 3. The larger the ratio of two factors, the more important the former factor is relative to the latter factor. In addition, the ratio of importance between the two factors is reciprocal to each other, where $b_{jk} = 1/b_{kj}$, $b_{jj} = 1$, $j, k = 1,\ldots, N$. The RI (Random Index) is an experimental value which depends on nc.

TABLE 2. Judgments matrix B.

A_i	B_1	B_2	...	B_N
B_1	b_{11}	b_{12}	...	b_{1N}
B_2	b_{21}	b_{22}	...	b_{2N}
...	...	...	...	...
B_N	b_{N1}	b_{N1}	...	b_{NN}

The CR (Consistency Ratio) of matrix B is used to check judgment inconsistencies. $CR = CI/RI$, where $CI = (\lambda_{max} - N) / (N - 1)$ and λ_{max} is the maximal eigenvalue of judgments matrix B. Given the matrix B and eigenvalue λ, the eigenvectors w_a satisfy the relationship that $B \cdot w_a = \lambda \cdot w_a$. The normalized eigenvectors W, according to the maximum eigenvalue λ_{max}, is the weight vector for AHP criteria or indexes.

As an acceptable consistency of the judgment matrix, $CR < 0.10$, which means the weights of decision maker are reasonable.

TABLE 3. Saaty's fundamental scale.

RI	nc	Definition
0	1	Equal importance/preference
0	2	Weak
0.58	3	Moderate importance/preference
0.90	4	Moderate plus
1.12	5	Strong importance/preference
1.24	6	Strong plus
1.32	7	Very strong or demonstrated importance/preference
1.41	8	Very, very strong
1.45	9	Extreme importance/preference

TABLE 4. Judgments matrix C_{static} for path smoothness $B_{1static}$.

$B_{1static}$	$C_{1static}$	$C_{2static}$	$C_{3static}$	$C_{4static}$	W	
$C_{1static}$	1	1/7	1/5	1/3	0.0553	λ_{max}=4.1170
$C_{2static}$	7	1	3	5	0.5650	CI=0.0390
$C_{3static}$	5	1/3	1	3	0.2622	RI=0.90
$C_{4static}$	3	1/5	1/3	1	0.1175	CR=0.0433 <0.10

3) SINGLE LAYER EVALUATION

For path decision maker, the criteria are smoothness $B_{1static}$ and economy $B_{2static}$. Since the smoothness of the path directly affects the ride smoothness of vehicles, the smoother the path is, the more the actual tracked path conforms to the desired path. Therefore, the smoothness of the path is more important than the economy. The ratio of the criteria is set as:

$$B_{1static} : B_{2static} = 3 : 1 = 0.75 : 0.25 \tag{14}$$

Down to the indexes layer as shown in Fig.18(a), a judgment matrix C_{static} is firstly established to evaluate the smoothness $B_{1static}$ of the path, as the smaller the change in curvature, the smoother the path. The sum of curvature squared κ_g represents the total of steering angle, the sum of squared derivation of curvature $d\kappa_g$ illustrates the total amount of change in steering, and the lateral offset from reference path l_{off} affects the lateral offset of the reference path. The above three factors have obvious effects on smoothness relative to path length S_g, and the importance relationship of the four factors is: sum of curvature squared $C_{2static}$ > sum of squared derivation of curvature $C_{3static}$ > lateral offset from reference path $C_{4static}$ > path length $C_{1static}$. The judgment matrix and corresponding calculation results are listed in Table 4. The CR (Consistency Ratio) of matrix C_{static} for path smoothness $B_{1static}$ is 0.0433 < 0.10, which means the sorting is reasonable.

TABLE 5. Judgments matrix C_{static} for path smoothness $B_{2static}$.

$B_{2static}$	$C_{1static}$	$C_{2static}$	$C_{3static}$	$C_{4static}$	W	
$C_{1static}$	1	3	5	4	0.5462	λ_{max}=4.0512
$C_{2static}$	1/3	1	3	2	0.2323	CI=0.0170
$C_{3static}$	1/5	1/3	1	1/2	0.0838	RI=0.90
$C_{4static}$	1/4	1/2	2	1	0.1377	CR=0.0189 <0.10

TABLE 6. Judgments matrix $B_{dynamic}$ for optimal trajectory $A_{dynamic}$.

$A_{dynamic}$	$B_{1dynamic}$	$B_{2dynamic}$	$B_{3dynamic}$	W	
$B_{1dynamic}$	1	2	3	0.5396	λ_{max}=3.0092
$B_{2dynamic}$	1/2	1	2	0.2970	CI=0.0046
$B_{3dynamic}$	1/3	1/2	1	0.1634	RI=0.58
					CR=0.0079 <0.10

As shown in Fig.18(a), a judgment matrix C_{static} is secondly established to evaluate the economy $B_{2static}$ of the path, which means the shorter the path length, the more economical it is. The path length l_{off} is directly related to the mileage traveled by the vehicle, so it has the greatest impact force. Secondly, if the sum of curvature squared κ_g is larger, the path is more curved, which means the path to be executed is longer. It can be considered that grounding between them reduces economy. And it is considered that the sum of squared derivation of curvature $d\kappa_g$ and the lateral offset from reference path l_{off} have minimal influence on the economy. Finally, ranging the importance of the four factors is: path length $C_{1static}$ > sum of curvature squared $C_{2static}$ > lateral offset from reference path $C_{4static}$ > sum of squared derivation of curvature $C_{3static}$. The judgment matrix and corresponding calculation results are listed in Table 5. The CR of matrix C_{static} for path smoothness $B_{2static}$ is 0.0189 < 0.10, which means the sorting is reasonable.

For trajectory decision maker, the criteria are smoothness $B_{1dynamic}$, comfortableness $B_{2dynamic}$ and economy $B_{3dynamic}$. The smoothness of the trajectory is mainly related to the curvature factor, which means it is directly related to the steering radius of the vehicle when vehicle tracks trajectory, and then it will affect the lateral force on the wheel and the smoothness of the steering wheel, further on, it challenges safety of vehicle. Therefore, smoothness is the most important over the other factors. Secondly, it is considered that the comfort of passengers should be given priority to by people, and be ranked before the cost. Therefore, the importance of the three performances is as follows: smoothness $B_{1dynamic}$ > comfortableness $B_{2dynamic}$ > economy $B_{3dynamic}$. And the judgment matrix is listed in Table 6. The $CR = 0.0189 <$ 0.10 means the rank is reasonable.

Then, the importance of each indexes in the indexes layer is analyzed around the three criteria of the trajectory. The first is smoothness $B_{1dynamic}$, which is like the $B_{1static}$ in path decision maker. The sum of curvature squared κ_g, sum of squared derivation of curvature $d\kappa_g$ and lateral offset from reference path l_{off} are the main factors affecting the smoothness of the path, and the second is the peak lateral acceleration a_{ymax} mainly caused by steering the front wheel of the vehicle. In addition, for the same lateral offset from reference path l_{off}, the longer the path length S_g is, the smoother the path is. For total of time consumed for trajectory execution t_g, sum of longitude acceleration squared a_g and sum of squared derivation of longitude acceleration da_g, it is considered that these three factors have little influence on the smoothness. Finally, the importance rank of eight indexes is: sum of curvature squared $C_{2dynamic}$ > sum of squared derivation of curvature $C_{3dynamic}$ > lateral offset from reference path $C_{4dynamic}$ > peak lateral acceleration $C_{8dynamic}$ > path length $C_{1dynamic}$ > total of time consumed for trajectory execution $C_{5dynamic}$ = sum of longitude acceleration squared $C_{6dynamic}$ = sum of squared derivation of longitude acceleration $C_{7dynamic}$. And the judgment matrix is listed in Table 7. The $CR = 0.0313 < 0.10$ means the rank is sound.

The comfortableness of riding is mainly determined by the human body's response to the vibration of the vehicle. The amplitude, frequency, position, direction and time of vehicle vibration will affect the subjective perception of human body. In general, the influence of vibration on human comfort and health can be directly evaluated by the mean root value of total weighted acceleration. Therefore, in the above eight evaluation indexes, acceleration-related indexes will play a major role in influencing comfort. Secondly, curvature correlation index and lateral offset from reference path l_{off} will have an impact on the lateral motion of vehicles. In this paper, the influence of these three indexes is secondary to that of acceleration correlation indexes. In lane changing and steering conditions, the travel time and path length are usually not in the same order of magnitude as the uncomfortable time and path length. Therefore, it considers that these two indexes have little influence. Finally, the importance sort of the eight indicators is: the importance rank of eight indexes is: sum of longitude acceleration squared $C_{6dynamic}$ > peak lateral acceleration $C_{8dynamic}$ > sum of squared derivation of longitude acceleration $C_{7dynamic}$ > sum of curvature squared $C_{2dynamic}$ > sum of squared derivation of curvature $C_{3dynamic}$ > lateral offset from reference path $C_{4dynamic}$ > total of time consumed for trajectory execution $C_{5dynamic}$ > path length $C_{1dynamic}$. And the judgment matrix is listed in Table 8. The $CR = 0.0361 < 0.10$ means the rank is sound.

For evaluating the economy of the trajectory, driving distance and total time are the most important factors affecting energy consumption. Since vehicle acceleration, deceleration, braking and other working conditions will also affect energy consumption, the influence degree of indicators related to acceleration is only second to distance and time. In general, the shorter the distance between the target point and the reference target point, the shorter the calculated path length is, so the influence is greater than the curvature related factors. The importance of eight indexes is: path length $C_{1dynamic}$ > total of time consumed for trajectory execution $C_{5dynamic}$ > sum of longitude acceleration squared $C_{6dynamic}$ > sum of squared derivation of longitude acceleration $C_{7dynamic}$ > peak lateral acceleration $C_{8dynamic}$ > lateral

TABLE 7. Judgments matrix $C_{dynamic}$ for trajectory smoothness $B_{1dynamic}$.

$B_{1dynamic}$	$C_{1dynamic}$	$C_{2dynamic}$	$C_{3dynamic}$	$C_{4dynamic}$	$C_{5dynamic}$	$C_{6dynamic}$	$C_{7dynamic}$	$C_{8dynamic}$	W	
$C_{1dynamic}$	1	1/8	1/6	1/4	2	2	2	1/2	0.0460	
$C_{2dynamic}$	8	1	3	5	9	9	9	7	0.4175	
$C_{3dynamic}$	6	1/3	1	3	7	7	7	5	0.2438	λ_{max}=8.3091
$C_{4dynamic}$	4	1/5	1/3	1	5	5	5	3	0.1350	CI=0.0442
$C_{5dynamic}$	1/2	1/9	1/7	1/5	1	1	1	1/3	0.0291	RI=1.41
$C_{6dynamic}$	1/2	1/9	1/7	1/5	1	1	1	1/3	0.0291	CR=0.0313<0.10
$C_{7dynamic}$	1/2	1/9	1/7	1/5	1	1	1	1/3	0.0291	
$C_{8dynamic}$	2	1/7	1/5	1/3	3	3	3	1	0.0695	

TABLE 8. Judgments matrix $C_{dynamic}$ for trajectory comfortableness $B_{2dynamic}$.

$B_{2dynamic}$	$C_{1dynamic}$	$C_{2dynamic}$	$C_{3dynamic}$	$C_{4dynamic}$	$C_{5dynamic}$	$C_{6dynamic}$	$C_{7dynamic}$	$C_{8dynamic}$	W	
$C_{1dynamic}$	1	1/5	1/4	1/3	1/2	1/9	1/7	1/8	0.0210	
$C_{2dynamic}$	5	1	2	3	4	1/5	1/3	1/4	0.0887	
$C_{3dynamic}$	4	1/2	1	2	3	1/6	1/4	1/5	0.0607	λ_{max}=8.3564,
$C_{4dynamic}$	3	1/3	1/2	1	2	1/7	1/5	1/6	0.0414	CI=0.0509,
$C_{5dynamic}$	2	1/4	1/3	1/2	1	1/8	1/6	1/7	0.0288	RI=1.41,
$C_{6dynamic}$	9	5	6	7	8	1	3	2	0.3429	CR=0.0361<0.10
$C_{7dynamic}$	7	3	4	5	6	1/3	1	1/2	0.1728	
$C_{8dynamic}$	8	4	5	6	7	1/2	2	1	0.2437	

TABLE 9. Judgments matrix $C_{dynamic}$ for Trajectory Economy $B_{3dynamic}$.

$B_{3dynamic}$	$C_{1dynamic}$	$C_{2dynamic}$	$C_{3dynamic}$	$C_{4dynamic}$	$C_{5dynamic}$	$C_{6dynamic}$	$C_{7dynamic}$	$C_{8dynamic}$	W	
$C_{1dynamic}$	1	9	9	7	2	3	4	5	0.3331	
$C_{2dynamic}$	1/9	1	1	1/3	1/8	1/7	1/6	1/5	0.0214	
$C_{3dynamic}$	1/9	1	1	1/3	1/8	1/7	1/6	1/5	0.0214	λ_{max}=8.3703
$C_{4dynamic}$	1/7	3	3	1	1/6	1/5	1/4	1/3	0.0409	CI=0.0529
$C_{5dynamic}$	1/2	8	8	6	1	2	3	4	0.2335	RI=1.41
$C_{6dynamic}$	1/3	7	7	5	1/2	1	2	3	0.1611	CR=0.0375<0.10
$C_{7dynamic}$	1/4	6	6	4	1/3	1/2	1	2	0.1110	
$C_{8dynamic}$	1/5	5	5	3	1/4	1/3	1/2	1	0.0776	

offset from reference path $C_{4dynamic}$ > sum of curvature squared $C_{2dynamic}$ = sum of squared derivation of curvature $C_{3dynamic}$. And the judgment matrix is listed in Table 9. The $CR = 0.0375 < 0.10$ means the rank is valid.

4) COMPREHENSIVE EVALUATION

The weights of all elements in the criterion layer and each element in the indexes layer can be calculated according to the results of single layer evaluation.

It is assumption that for the criteria layer $B_1, \ldots, B_m$, the calculated weight is $b_1, \ldots, b_m$. And the corresponding indexes layer of the element B_i is $C_1, \ldots, C_n$, the calculated weight is $c_1^i, \ldots, c_n^i$, so the comprehensive weight of index C_j can be obtained as follows:

$$\omega_j = \sum_{i=1}^{m} b_i c_j^i \tag{15}$$

For path decision maker, the comprehensive weight of indexes is listed in Table 10 and the comprehensive weight of indexes is listed in Table 11 for trajectory decision maker.

The CR (Consistency Ratio) for comprehensive weight of indexes is:

$$CR = \frac{CI}{RI} = \frac{\sum_{i=1}^{m} (b_i \cdot CI_i)}{\sum_{i=1}^{m} (b_i \cdot RI_i)} \tag{16}$$

TABLE 10. Comprehensive weight of indexes for path.

Criteria/ indexes	$B_{1static}$	$B_{2static}$	Index weight
	0.7500	0.2500	
$C_{1static}$	0.0553	0.5462	0.1780
$C_{2static}$	0.5650	0.2323	0.4818
$C_{3static}$	0.2622	0.0838	0.2176
$C_{4static}$	0.1175	0.1377	0.1226

TABLE 11. Comprehensive weight of indexes for trajectory.

Criteria/indexes	$B_{1dynamic}$	$B_{2dynamic}$	$B_{3dynamic}$	Index weight
	0.5396	0.2970	0.1634	
$C_{1dynamic}$	0.0460	0.0210	0.3331	0.0855
$C_{2dynamic}$	0.4175	0.0887	0.0214	0.2551
$C_{3dynamic}$	0.2438	0.0607	0.0214	0.1531
$C_{4dynamic}$	0.1350	0.0414	0.0409	0.0923
$C_{5dynamic}$	0.0291	0.0288	0.2335	0.0624
$C_{6dynamic}$	0.0291	0.3429	0.1611	0.1439
$C_{7dynamic}$	0.0291	0.1728	0.111	0.0852
$C_{8dynamic}$	0.0695	0.2437	0.0776	0.1225

TABLE 12. Consistency of the judgment matrix for path.

Components	$B_{1static}$	$B_{2static}$	
b_i	0.7500	0.2500	CR=0.0372<0.10
CI_i	0.0390	0.0170	
RI_i	0.9000	0.9000	

TABLE 13. Comprehensive weight of indexes for trajectory.

Components	$B_{1dynamic}$	$B_{2dynamic}$	$B_{3dynamic}$	
b_i	0.5396	0.2970	0.1634	CR=0.0338 <0.10
CI_i	0.0442	0.0509	0.0529	
RI_i	1.4100	1.4100	1.4100	

where, CI_i and RI_i are the consistency index and random consistency index of the indexes layer corresponding to the element coefficient b_i of the criteria layer respectively.

The results of path decision maker and trajectory decision maker are listed in Table 12 and Table 13, respectively. The *CR* of path decision maker and trajectory decision maker are less than 0.1, which indicates that the *HAHP* decision maker conforms to the design requirements.

IV. EXPERIMENTAL RESULTS AND ANALYSIS

To make the simulation test closer to the real situation, a joint simulation system based on *visual studio* 2013, *Matlab/Simulink, Carsim* and *Prescan* in *windows10* is designed, as shown in Fig.19, of which the processor is 1.80 GHz Intel® Core™i5-8250U with 7.86GB of memory.

The real vehicle platform is developed based on *E50 electric vehicle* with *drive-by-wire*, *brake-by-wire* and *steer-by-wire*, which embedded *RT3003/PDL* system as high accuracy positioning navigator and *ARK-3500* as code runner. As shown in Fig.20, a *hierarchical motion controller* [42], [43] is developed to track reference trajectory

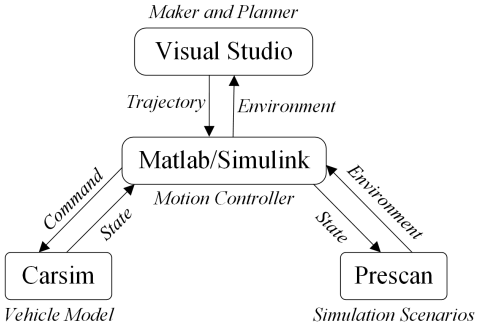

FIGURE 19. Joint simulation system.

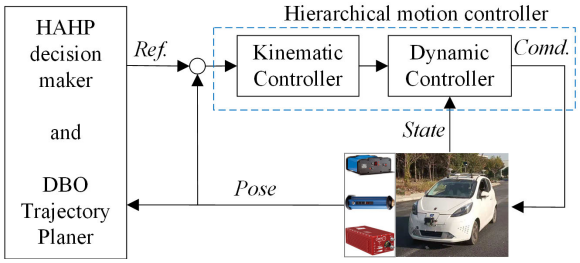

FIGURE 20. Real vehicle platform.

TABLE 14. Key parameters for testing.

Parameter	Value
Wheel base/m	2.305
vehicle length/m	3.569
vehicle width/m	1.551
Distance from rear axle to front/m	3.069
Maximum speed/(m/s)	20
Maximum acceleration/(m/s^2)	2
Maximum deceleration/(m/s^2)	-8
Maximum lateral acceleration/(m/s^2)	3.92
Maximum curvature/m^{-1}	0.25

generated by *HAHP decision maker* and *DBO trajectory planner*. The key parameters for testing are listed in Table 14.

A. SIMULATION TESTS

To verify the real-time performance and safety of the algorithm, seven typical scenarios (*Scenario A to Scenario G*) of lane changing for obstacle avoidance and turn are designed, and the mean time consumption of 1000 cycles in each scenario are employed as evaluation index.

Scenario A is a left lane changing in double drive lane as avoiding a static obstacle shown in Fig.21. The vehicle goes straight with 32 km/h and a static obstacle (the black box in Fig.21(a)) is located 16 m in the front of the vehicle direction lane, which compels the vehicle changing left to avoid collision. The blue stars in Fig.21(a) are safety nodes of 25 candidate path set after collision checking. After eliminating the 19 unsafe paths by collision detection, candidate trajectory set could be obtained by velocity planning for the

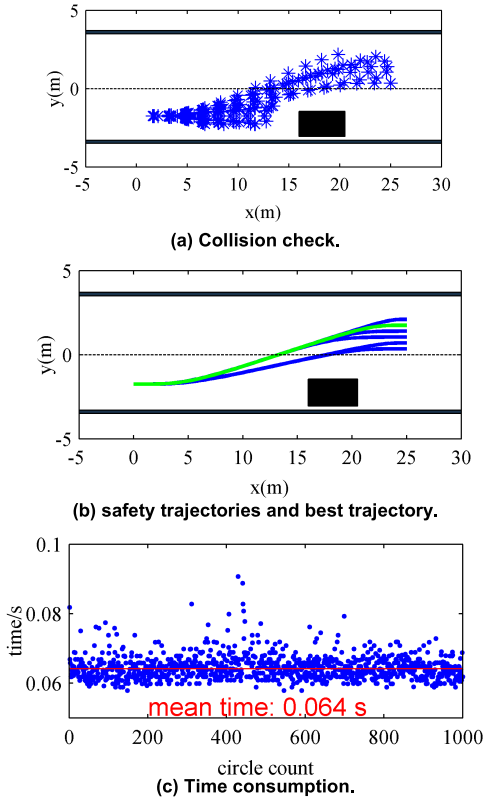

FIGURE 21. *Scenario A*: single obstacle avoidance in double lane.

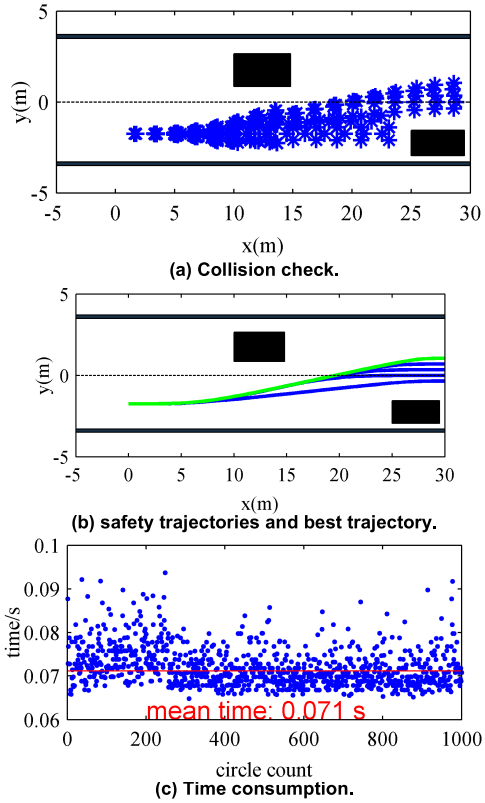

FIGURE 22. *Scenario B*: double obstacle avoidance in double lane.

remaining paths as the 6 blue curves shown in Fig.21(b). Then the green curve in Fig.21(b) is best trajectory proceeding out of *HAHP* decision maker. Finally, the time consumption of 1000 circles test is depicted in Fig.21(c), where the mean-time is 0.064s ($\leq$0.1s) and the maximum time is 0.0907s ($\leq$0.1s).

Expand to more general, *Scenario B* is a left lane changing in double drive lane causes as avoiding two static obstacles shown in Fig.22. The vehicle goes straight with 37 km/h and two static obstacles (the black box in Fig.22(a)) is located 10 m and 25m in the front of the vehicle, which compels the vehicle changing left lane to avoid obstacles. The blue stars in Fig.22(a) are safety nodes of 25 path set after collision checking. After deleting the 20 unsafe paths, the blue curves shown in Fig.22(b) are 5 candidate trajectories and the green one is best trajectory, which is derived from *HAHP* decision maker. As shown in Fig.22(c), the meantime of 1000 circles is 0.071s and the maximum is 0.0937s, which has 0.009s and 0.003s rising up compared with *Scenario A* since the *Scenario B* is more complicated. However, both meantime and maximum are under 0.1s level.

As depicted in Fig.23, *Scenario C* is a scenario of a lane changing in three drive lane. The vehicle goes straight with 15 km/h in middle line and three static obstacles (the black box in Fig.23(a)) is located 6 m 15m and 25m in the front of the vehicle, which compels the vehicle changing right lane to avoid obstacles. After collision checking for 25 candidate path set, the safety nodes are the blue stars in Fig.23(a). Then, there are 4 safety paths for planning velocity to generate candidate trajectories as the blue splines shown in Fig.23(b). Finally, the green trajectory in Fig.23(b) is the best trajectory, which is produced by *HAHP* decision maker. As depicted in Fig.23(c), the mean time for 1000 circles is 0.098s and the max time is 0.1297s, which has 0.027s and 0.036s rising compared with *Scenario B* since the *Scenario C* is more complex. However, the meantime is under 0.1s level.

As depicted in Fig.23, *Scenario D* is a scenario of turn left for two-lane intersection in both directions. At a speed of 15km/h, the vehicle prepares to turn left in the right lane. The target position is the left-turn lane with a longitudinal position of 18m and a transverse position of $-$15m, and the target speed is 13km/h. Although there are no obstacles, the planned path should avoid overlap with the lane lines, therefore the lane lines are virtual obstacles. After collision checking for 20 candidate path set, the safety nodes are the blue stars in Fig.24(a). Then, there are 3 safety paths for planning velocity to generate candidate trajectories as the blue splines shown in Fig.24(b). Finally, the green trajectory in Fig.24(b) is the best trajectory, which is selected out by *HAHP* decision maker. As depicted in Fig.24(c), the mean time for 1000 circles is 0.087s and the max time is 0.0974s, where both meantime and max time are under 0.1s level.

Scenario E is a scenario of turn left for two-lane intersection in both directions with a static obstacle. Except for

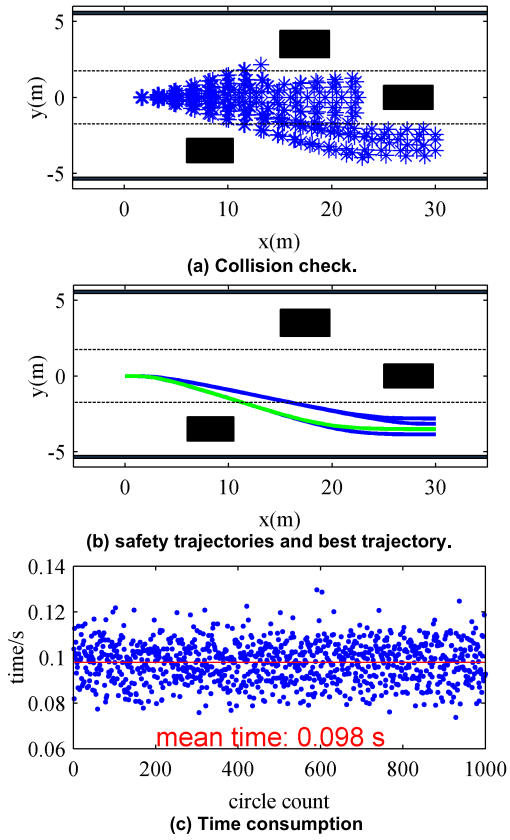

FIGURE 23. *Scenario C*: three obstacle avoidance in three lanes.

adding an obstacle, other conditions are set to the same as *Scenario D*. Like Fig.24(a), after collision checking for 20 candidate path set, the safety nodes are the blue stars in Fig.25(a). Then, there are and only are one safety path for planning velocity to generate candidate trajectories as the green spline shown in Fig.25(b). Finally, the green trajectory is the best trajectory, which is picked out by *HAHP* decision maker. As depicted in Fig.25(c), the mean time for 1000 circles is 0.076s and the max time is 0.0918s, which has 0.011s and 0.0056s reducing compared with *Scenario D*, since the *Scenario E* has and only has one path for planning velocity. However, both meantime and max time are under 0.1s level.

As shown in Fig.26, *Scenario F* is a scenario of turn right for two-lane intersection in both directions. At a speed of 15km/h, the vehicle prepares to turn right in the right lane. The target position is the right-turn lane with a longitudinal position of 11m and a transverse position of 10m, and the target speed is 15km/h. Similar with *Scenario D*, the planned path should avoid overlap with the lane lines, therefore the lane lines are virtual obstacles. After collision checking for 20 candidate path set, the safety nodes are the blue stars in Fig.26(a). Then, there are 3 safety paths for planning velocity to generate candidate trajectories as the blue splines shown in Fig.26(b). Finally, the green trajectory in Fig.26(b) is the best trajectory, which is sorted out by *HAHP* decision maker. As depicted in Fig.26(c), the mean time for 1000 circles is

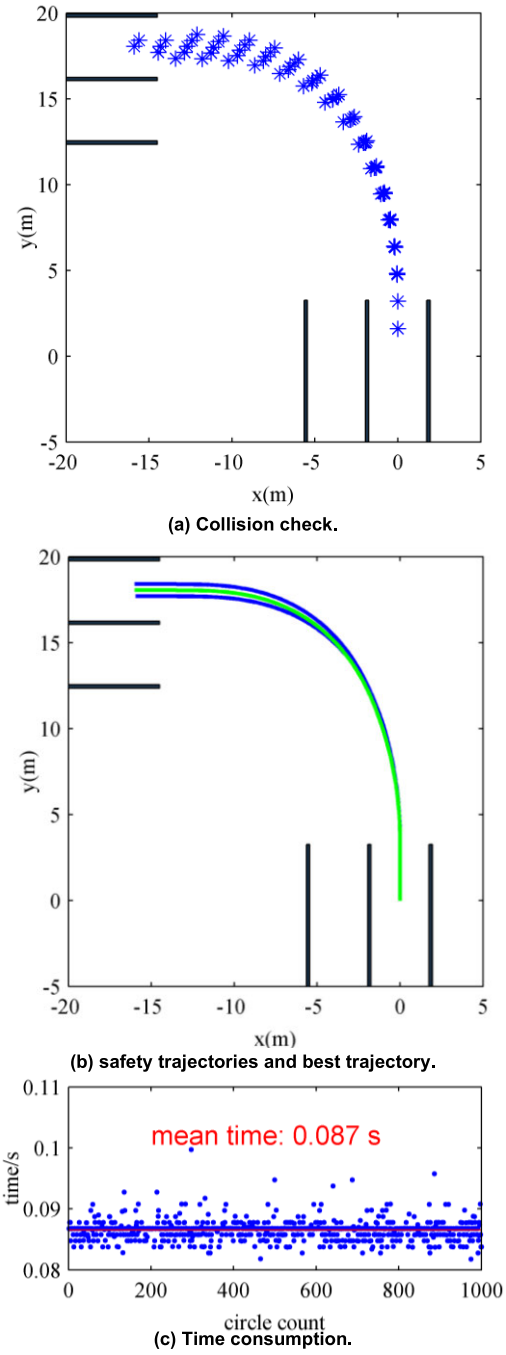

FIGURE 24. *Scenario D*: no obstacle avoidance for turning left.

0.065s and the max time is 0.0928s, where both meantime and max time are under 0.1s level.

Scenario G is a scenario of turn right for two-lane intersection in both directions with a static obstacle. Except for adding an obstacle, other conditions are set to the same as *Scenario F*. Similar with Fig.26(a), after collision checking for 20 candidate path set, the safety nodes are the blue stars in Fig.27(a). Then, there are and only are one safety path for planning velocity to generate candidate trajectories as the green spline shown in Fig.27(b). Finally, the green trajectory

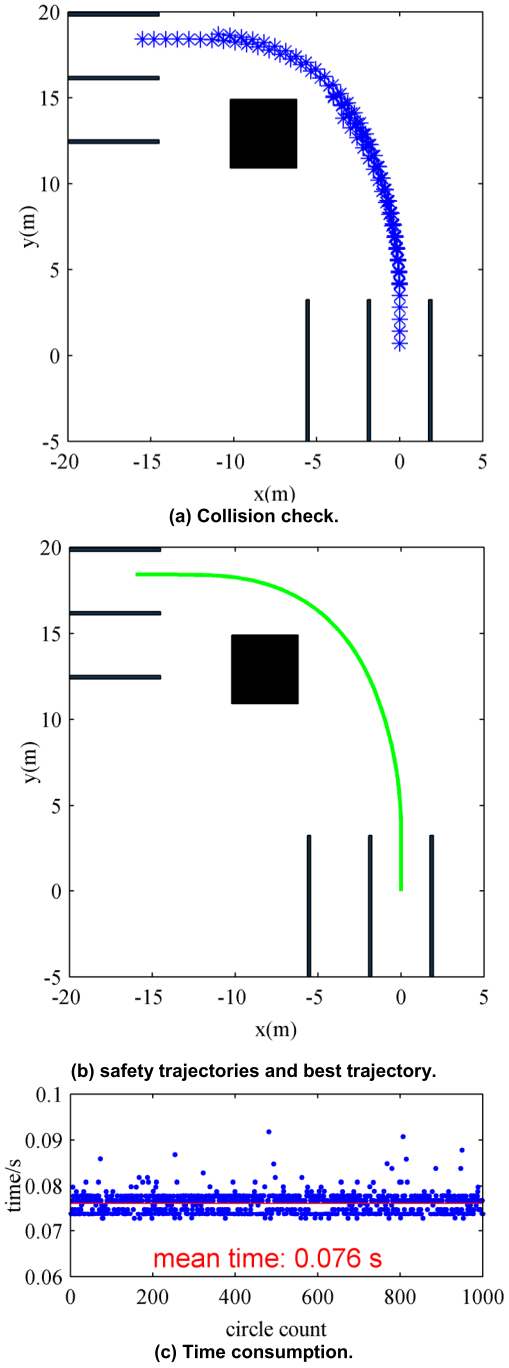

FIGURE 25. *Scenario E*: single obstacle avoidance for turning left.

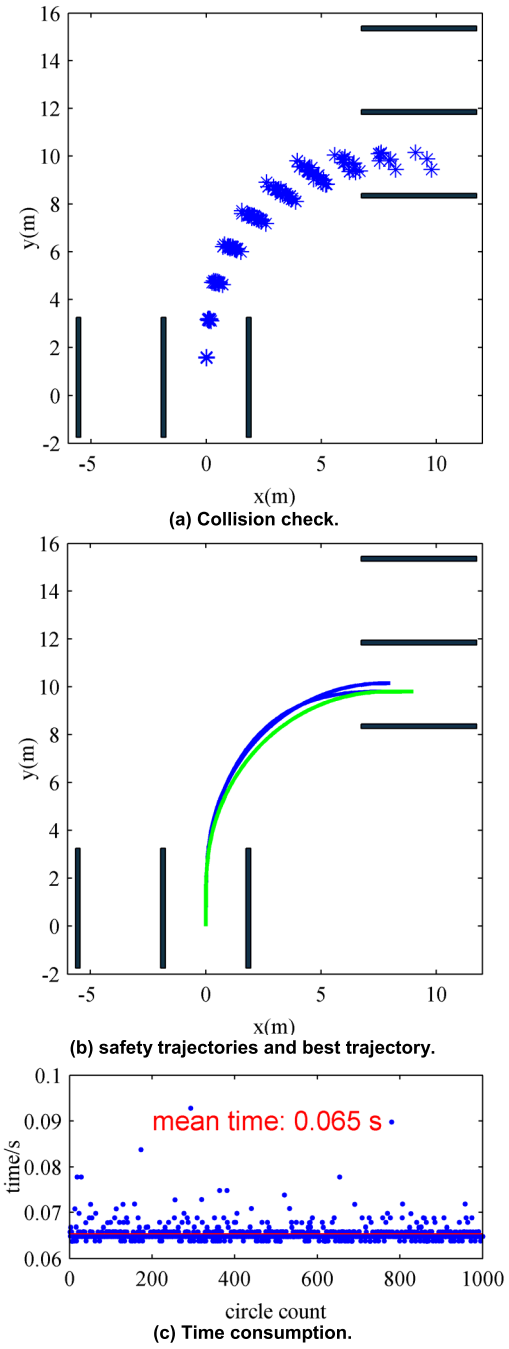

FIGURE 26. *Scenario F*: no obstacle avoidance for turning right.

is the best trajectory, which is stemmed from *HAHP* decision maker. As depicted in Fig.27(c), the mean time for 1000 circles is 0.063s and the max time is 0.0958s, which has 0.002s reducing of mean time and 0.0039s rising up of max time compared with *Scenario F*, since the *Scenario G* has and only has one path for planning velocity. However, both meantime and max time are under 0.1s level.

To further evaluate the stability of the design algorithm, it is employed *three sigma*(3σ) criterion and *six sigma*(6σ) criterion, which are prevalent criteria for process improvement in *Statistical Process Control* (*SPC*) [44]–[46]. In business applications, *three sigma*(3σ)/*six sigma*(6σ) refer to processes that operate efficiently and stably and produce items of the highest quality. In *SPC*, there is an *Upper Control Limit* (*UCL*) and a *Lower Control Limit* (*LCL*) set. The *UCL* is set *three sigma*/*six sigma* levels above the mean and the LCL is set at *three sigma*/*six sigma* levels below mean. As shown in Fig.28, If the mass characteristic x is normally distributed, 99.73% of the mass characteristic is included in the 3σ range and 99.9999998% in the 6σ range.

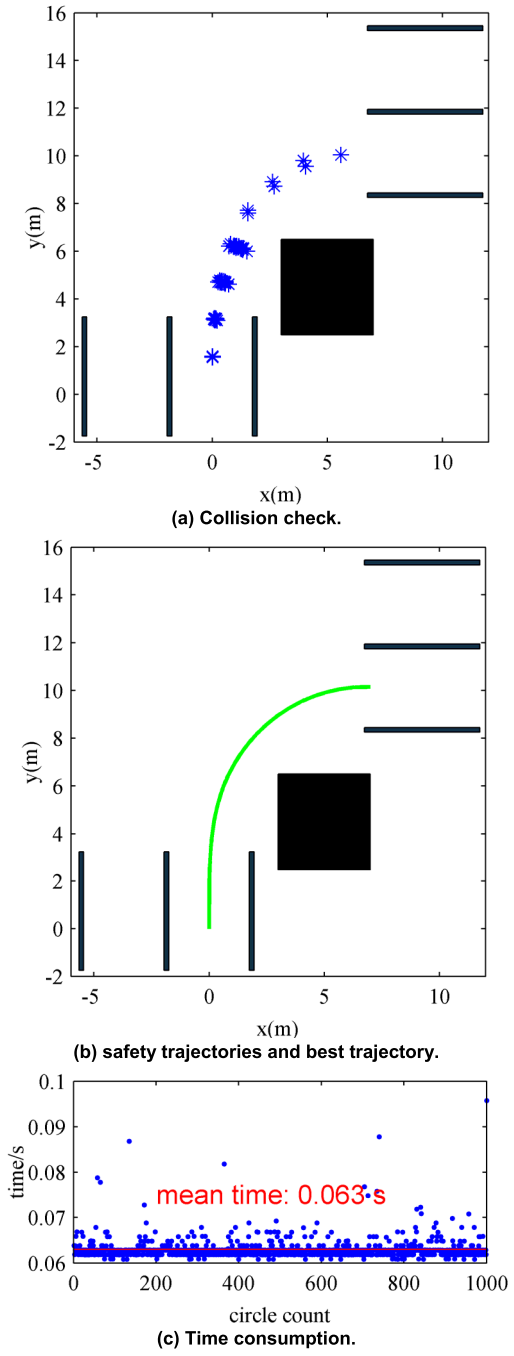

FIGURE 27. *Scenario G*: single obstacle avoidance for turning right.

The key statistical data and criteria for *Scenario A-G* are listed in Table 15. All the mean time (μ_t) are less than 0.1s and mean square error (σ_t) are less than 0.01s. The max time t_{max} is less than 0.1s except *Scenario C* is 0.1249s by employed *three sigma*(3σ) criterion. Similarly, the max time t_{max} is less than 0.1s except *Scenario C* is 0.1518s by employed *six sigma*(6σ) criterion. Finally, the probability $P(t \leq 0.1s)$ for the max time t_{max} less than 0.1s criterion is 100% except *Scenario C* is 59.31%, which the calculation of $P(t \leq 0.1s)$ is $P(t \leq 0.1s) = \Phi((0.1-\mu_t)/\sigma_t)$. The result illustrates that

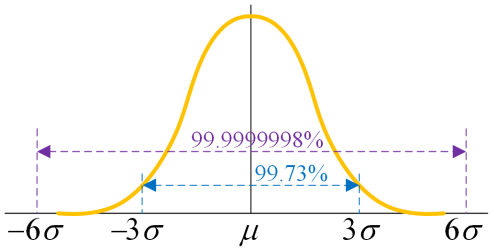

FIGURE 28. 3σ and 6σ for normal distribution.

TABLE 15. Key Data and Criteria for *Scenario A-G*.

Criteria	μ_t/s	σ_t/s	T_{max}/s (3σ)	T_{max}/s (6σ)	P ($t \leq 0.1s$)
Scenario A	0.0641	0.0036	0.0750	0.0858	100%
Scenario B	0.0712	0.0046	0.0851	0.0989	100%
Scenario C	0.0979	0.0090	0.1249	0.1518	59.31%
Scenario D	0.0865	0.0015	0.0909	0.0953	100%
Scenario E	0.0762	0.0021	0.0826	0.0890	100%
Scenario F	0.0654	0.0020	0.0714	0.0773	100%
Scenario G	0.0630	0.0024	0.0702	0.0773	100%

FIGURE 29. Real test zone.

TABLE 16. Key Errors of *Scenario H-L*.

Error/Scenario	*H*	*I*	*J*	*K*	*L*
Peak lateral/m	0.205	0.164	0.186	0.448	0.272
Mean lateral/m	0.106	0.071	0.089	0.174	0.108
Peak speed/(km/h)	1.488	1.493	1.010	0.350	0.380
Mean speed/(km/h)	0.374	0.297	0.499	0.087	0.101

the strategy of *HAHP decision maker* and *DBO trajectory planner* has high stability, although the performance of three obstacle avoidance in three lanes should be further improved.

B. REAL TESTS

All the real tests are completed in south of *the Proving Ground for ICVs of Tongji University* as depicted in Fig.29. According to joint simulation scenarios, 5 kinds of real vehicle test environments have been designed including 3 lane changing scenarios (*Scenario H to Scenario J*), 1 turn left scenario (*Scenario K*) and 1 turn right scenario (*Scenario L*).

As shown in Fig.30(a), the vehicle in *Scenario H* is forced to change to the left lane since the current lane has been

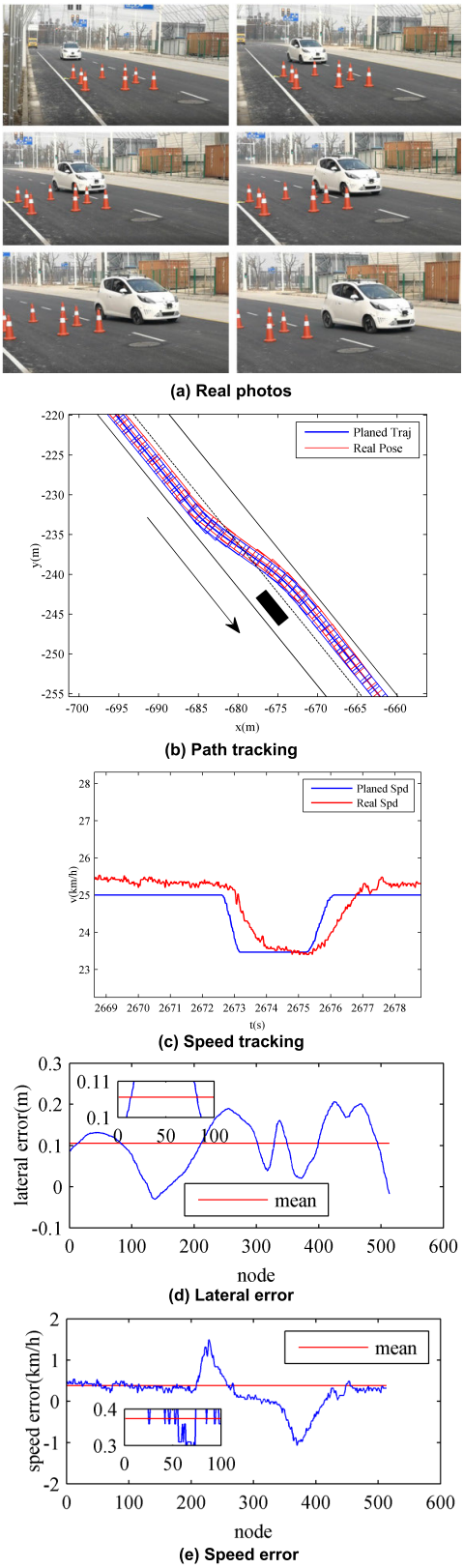

FIGURE 30. *Scenario H*: single obstacles avoidance in double lane.

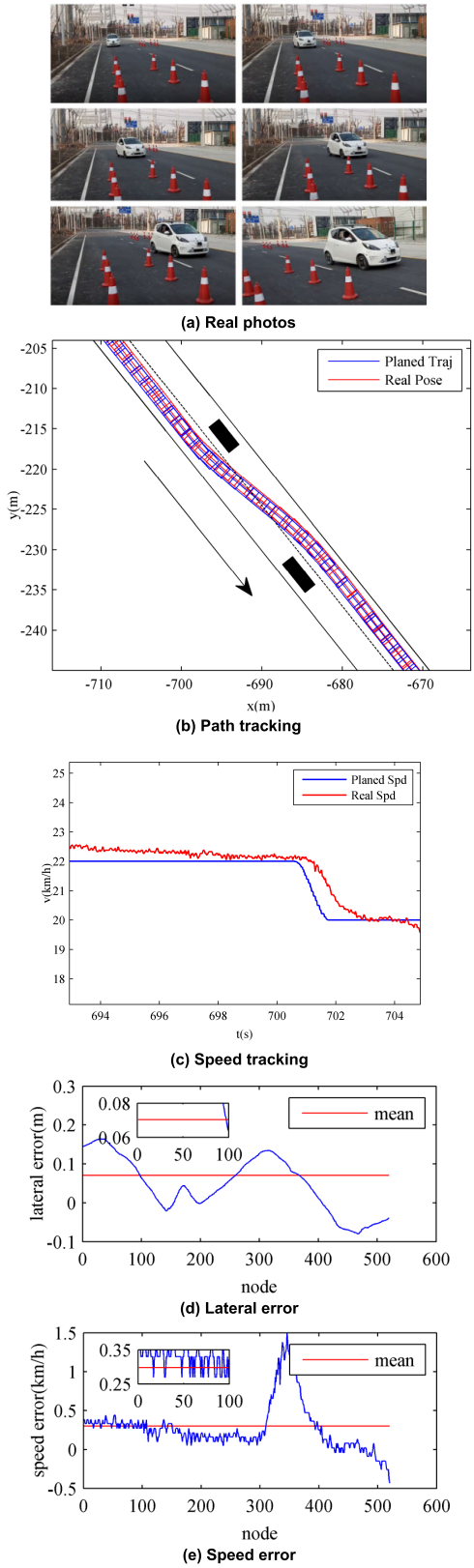

FIGURE 31. *Scenario I*: double obstacles avoidance in double lane.

occupied by a static obstacle located in position of 16m with 1.6 width. In Fig.30(b), the red part is the real-time positioning information read from *RTK3003*, the solid blue line and blue box are the planning module respectively to obtain the planning result and vehicle shape according to the real-time position, which the best trajectory is derived from *HAHP*

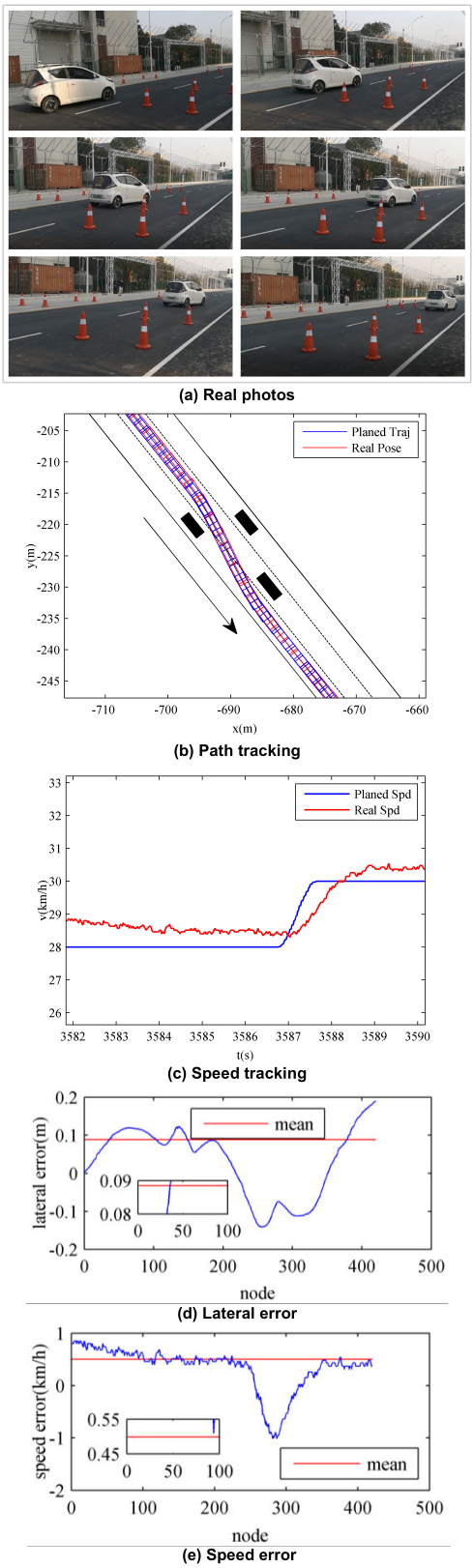

FIGURE 32. *Scenario J*: three obstacles avoidance in three lane.

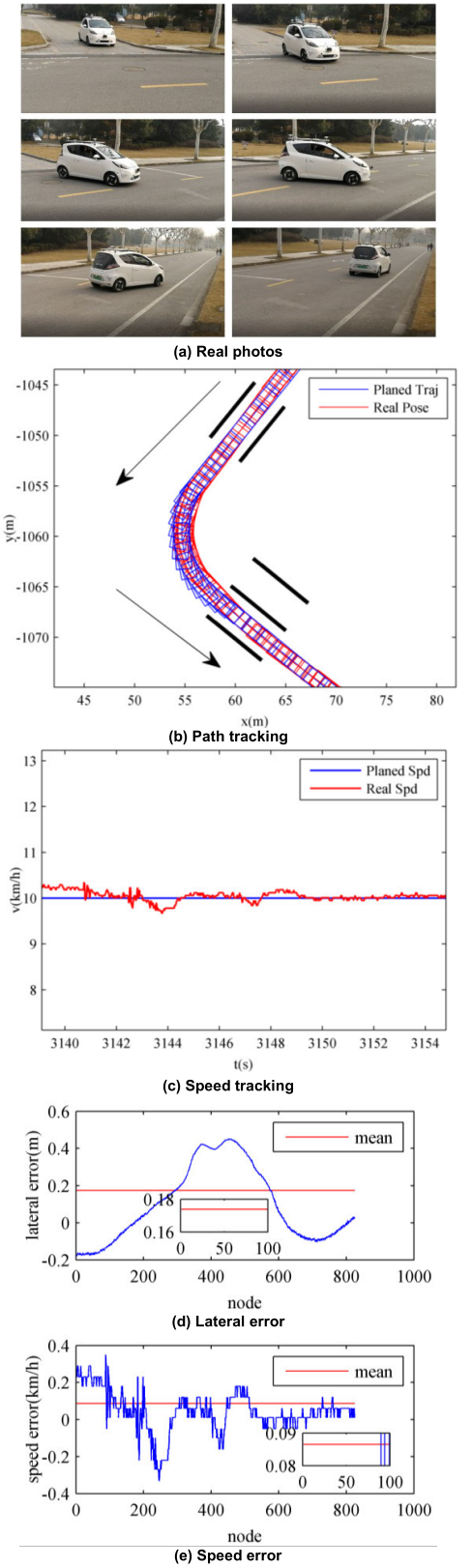

FIGURE 33. *Scenario K*: no obstacle avoidance for turning left.

decision maker. Both planned and real positions illustrated the vehicle could avoid obstacle. As the starting and target speeds given by the decision maker are both 25km/h, which is higher than the allowable speed of curvature in lane change, the planned velocity will be reduced to 23.47km/h, then kept the speed until closely changed to lift line, and accelerated

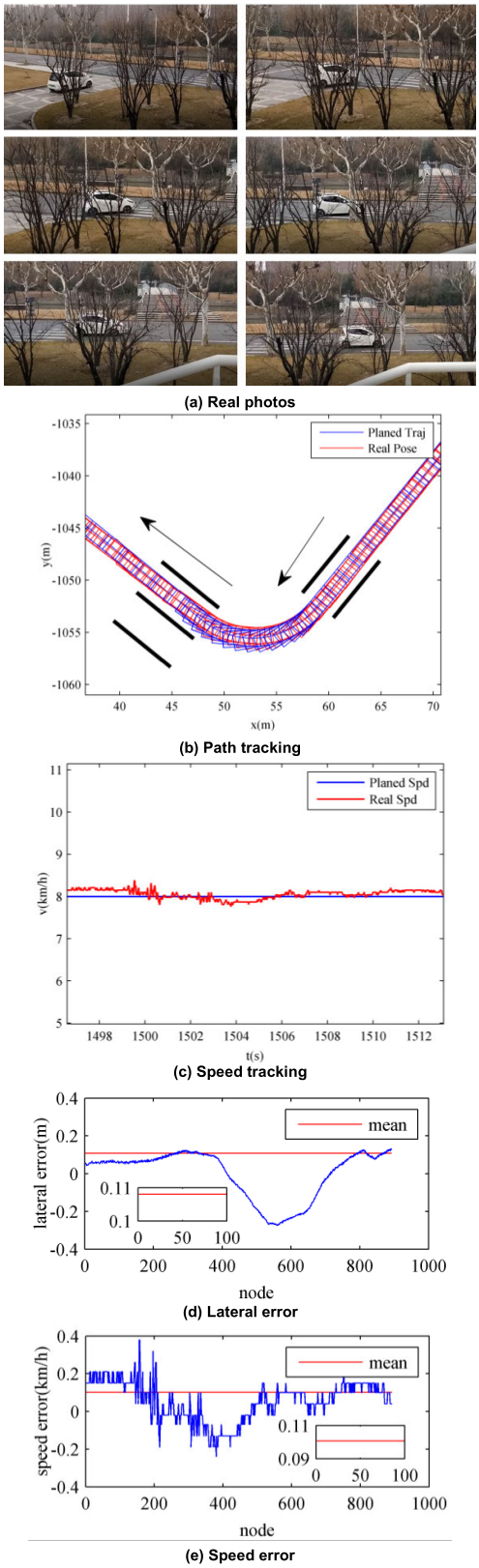

FIGURE 34. *Scenario L*: no obstacle avoidance for turning right.

to 25km/h as the blue curve shown in Fig.30(c). The lateral error is in [−0.0302, 0.2054]m and speed error in [−1.074, 1.488]km/h in Fig.30(d) and Fig.30(e), which means that the planned trajectory is smooth enough and satisfy the constraints of the actuator for keeping the performance of vehicle tracker.

Avoiding two obstacles in two drive lane scenario is shown in Fig.31(a). There is an obstacle with 1.6m width located in 22m in the front of vehicle at the current lane, and an obstacle with 1.8m width at the longitudinal distance 3m from the left lane. Fig.31(b) means the vehicle could avoid the two obstacles, which tracks the best trajectory stemmed from *HAHP* decision maker. The initial vehicle speed is 22km/h and the target vehicle speed is 20km/h. Since the planner has taken the constraints of the actuator into account, the lateral error is [−0.164, 0.079]m and speed error is [−0.43, 1.493]km/h.

Scenario J is designed for testing avoiding three obstacles in three drive lane as shown in Fig.32(a). There is a 4.8m length and 1.2m width obstacle at 20m longitudinal distance from the starting point of the current lane, an obstacle 4m length and 1.6m width at 5m longitudinal distance from the starting point of the right lane, and an obstacle 4.5m length and 1.6m width at 10m longitudinal distance from the starting point of the left lane (similar to the failed vehicle parked on the lane). Both planned and real pose are no intersection with obstructions and solid lane lines depicted in Fig.32(c), which means the best trajectory picked out by *HAHP* decision maker could successfully avoid obstacles. Meanwhile, the lateral error is [−0.142, 0.186]m and speed error is [−1.01, 0.85]km/h since the planned trajectory is smooth enough and satisfy the constraints of the actuator for vehicle tracking.

Scenario K in Fig.33 and *Scenario L* in Fig.34 are respectively no obstacle avoidance for turning left and right. As shown in Fig.33(b) and Fig.34(b), the solid blue line and blue box are the planning module respectively to obtain the planning result and vehicle shape according to the real-time position. Both planned and real positions are in one lane space, which illustrates the best trajectory selected out by *HAHP* decision maker could successfully turn left and right without collision. The lateral error of turning left is [−0.1745, 0.4481]m and the lateral error of turning right is [−0.272, 0.1335]m, and, respectively, speed error is [−0.33, 0.35]km/h and [−0.24, 0.38]km/h, which means that the planned trajectory is smooth enough and satisfy the constraints of the actuator for vehicle tracking.

V. CONCLUSION

For improving performance of intelligent vehicle driving on urban environment, a novel *driving behaviour oriented* (*DBO*) *trajectory planner* and *hierarchical analytic hierarchy process* (*HAHP*) *decision maker* are proposed in this paper.

Firstly, sparking in the traffic rules, the *DBO* framework is designed to plan safety lane changing and turning trajectory set. In order to make trajectory drivable, *cubic B-spline* and *clothoid curve* are parameterized to generate smooth path with continuous curvature, and *cubic polynomial curve* is employed to schedule velocity profile taking vehicle stability requirements, actuator constraints and comfort conditions into account.

Secondly, in order to pick out the best trajectory, *HAHP decision maker* is developed to evaluate the candidates. As the top layer, path decision maker selects optimal paths according to smoothness and economy by taking four static indexes in account. Then, trajectory decision maker, as the second layer, picks out best trajectory considering smoothness, comfortableness and economy by taking eight dynamic indexes in account.

Thirdly, it is embedded *DBO RRT path replanner* to make algorithm completeness. As guiding by the driving behavior, normal random, goal-bias and Gaussian sampling strategies are fused to reduce the randomness of node's extension to save the computation time.

Finally, both seven simulation and five real typical scenarios are designed to verify the performance of the algorithm.

Evaluated by *three sigma*(3σ) criterion and *six sigma*(6σ) criterion, the planner and maker have highly real-time performance and stability. Meanwhile, the final trajectory could address avoiding obstacles and actuator constraints as practical lateral and speed error for all scenarios.

Future work will focus on improving real time performance. And, the other research topic is to explore and build dynamic validation scenarios for matching the actual situation. Moreover, considering the driver's driving behavior is closely associated with the driving style, it is fruitful to develop multiple driving style *DBO* path planner. Furthermore, it would be worth considering the uncertainty of perception and actuators.

REFERENCES

[1] B. Paden, M. Čáp, S. Z. Yong, D. Yershov, and E. Frazzoli, "A survey of motion planning and control techniques for self-driving urban vehicles," *IEEE Trans. Intell. Veh.*, vol. 1, no. 1, pp. 33–55, Mar. 2016.

[2] SAE On-Road Automated Vehicle Standards Committee, "Taxonomy and definitions for terms related to driving automation systems for on-road motor vehicles," SAE Int., Warrendale, PA, USA, Tech. Rep. Ground Vehicle Standard J3016_201806, Jun. 2018, pp. 1–35.

[3] C. Katrakazas, M. Quddus, W.-H. Chen, and L. Deka, "Real-time motion planning methods for autonomous on-road driving: State-of-the-art and future research directions," *Transp. Res. C, Emerg. Technol.*, vol. 60, pp. 416–442, Nov. 2015.

[4] D. González, J. Pérez, V. Milanés, and F. Nashashibi, "A review of motion planning techniques for automated vehicles," *IEEE Trans. Intell. Transp. Syst.*, vol. 17, no. 4, pp. 1135–1145, Apr. 2016.

[5] S. M. LaValle and S. A. Hutchinson, "Optimal motion planning for multiple robots having independent goals," *IEEE Trans. Robot. Autom.*, vol. 14, no. 6, pp. 912–925, Dec. 1998.

[6] M. Likhachev and D. Ferguson, "Planning long dynamically feasible maneuvers for autonomous vehicles," *Int. J. Robot. Res.*, vol. 28, no. 8, pp. 933–945, 2009.

[7] E. A. Hansen and R. Zhou, "Anytime heuristic search," *J. Artif. Intell. Res.*, vol. 28, pp. 267–297, Mar. 2007.

[8] X. Sun, "Incremental ara*: An incremental anytime search algorithm for moving-target search," presented at the 22nd Int. Conf. Automat. Planning Scheduling, May 2012. [Online]. Available: https://www.aaai.org/ocs/index.php/ICAPS/ICAPS12/paper/view/4724/4735

[9] D. Ferguson and A. Stentz, "Using interpolation to improve path planning: The field D* algorithm," *J. Field Robot.*, vol. 23, no. 2, pp. 79–101, Mar. 2006.

[10] J. Petereit, "Application of hybrid A* to an autonomous mobile robot for path planning in unstructured outdoor environments," presented at the 7th German Conf. Robot., Munich, Germany, Sep. 2012. [Online]. Available: https://ieeexplore.ieee.org/stamp/stamp.jsp?tp=&arnumber=6309512

[11] T. Gu, "Focused trajectory planning for autonomous on-road driving," presented at the IEEE Intell. Vehicles Symp. (IV), Gold Coast, QLD, Australia, Jun. 2013. [Online]. Available: https://ieeexplore.ieee.org/stamp/stamp.jsp?tp=&arnumber=6629524

[12] L. Ma, J. Xue, K. Kawabata, J. Zhu, C. Ma, and N. Zheng, "Efficient sampling-based motion planning for on-road autonomous driving," *IEEE Trans. Intell. Transp. Syst.*, vol. 16, no. 4, pp. 1961–1976, Aug. 2015.

[13] S. M. LaValle, "Randomized kinodynamic planning," presented at the IEEE Int. Conf. Robot. Automat., Detroit, MI, USA, May 1999. [Online]. Available: https://ieeexplore.ieee.org/stamp/stamp.jsp?tp=&arnumber=770022

[14] L. E. Kavraki, P. Svestka, J.-C. Latombe, and M. H. Overmars, "Probabilistic roadmaps for path planning in high-dimensional configuration spaces," *IEEE Trans. Robot. Autom.*, vol. 12, no. 4, pp. 566–580, Aug. 1996.

[15] P. Sudhakara, V. Ganapathy, and K. Sundaran, "Optimal trajectory planning based on bidirectional spline-RRT* for wheeled mobile robot," presented at the 3rd Int. Conf. Sens., Signal Process. Secur., Chennai, India, May 2017. [Online]. Available: https://ieeexplore.ieee.org/stamp/stamp.jsp?tp=&arnumber=8071566

[16] C. Urmson and R. Simmons, "Approaches for heuristically biasing RRT growth," presented at the IEEE/RSJ Int. Conf. Intell. Robots Syst., Las Vegas, NV, USA, Oct. 2003. [Online]. Available: https://ieeexplore.ieee.org/stamp/stamp.jsp?tp=&arnumber=1248805

[17] M. Elbanhawi and M. Simic, "Randomised kinodynamic motion planning for an autonomous vehicle in semi-structured agricultural areas," *Biosyst. Eng.*, vol. 126, pp. 30–44, Oct. 2014.

[18] C. G. Keller, T. Dang, H. Fritz, A. Joos, C. Rabe, and D. M. Gavrila, "Active pedestrian safety by automatic braking and evasive steering," *IEEE Trans. Intell. Transp. Syst.*, vol. 12, no. 4, pp. 1292–1304, Apr. 2011.

[19] P. Petrov and F. Nashashibi, "Modeling and nonlinear adaptive control for autonomous vehicle overtaking," *IEEE Trans. Intell. Transp. Syst.*, vol. 15, no. 4, pp. 1643–1656, Aug. 2014.

[20] M. Brezak and I. Petrović, "Real-time approximation of clothoids with bounded error for path planning applications," *IEEE Trans. Robot.*, vol. 30, no. 2, pp. 207–515, Apr. 2014.

[21] D. Gonzáleza, J. Pérezb, and V. Milanés, "Parametric-based path generation for automated vehicles at roundabouts," *Expert Syst. Appl.*, vol. 71, pp. 332–341, Apr. 2017.

[22] U. Z. A. Hamid, M. H. M. Ariff, H. Zamzuri, Y. Saito, M. A. Zakaria, M. A. A. Rahman, and P. Raksincharoensak, "Piecewise trajectory replanner for highway collision avoidance systems with safe-distance based threat assessment strategy and nonlinear model predictive control," *J. Intell. Robot. Syst.*, vol. 90, nos. 3–4, pp. 363–385, Jun. 2018.

[23] F. von Hundelshausen, M. Himmelsbach, F. Hecker, A. Mueller, and H.-J. Wuensche, "Driving with tentacles: Integral structures for sensing and motion," *J. Field Robot.*, vol. 25, no. 9, pp. 640–673, 2008.

[24] M. Zhang and K. Zhang, "Improved execution method of tentacle algorithm for intelligent vehicle," *Trans. Nanjing Univ. Aeronaut. Astronaut. (English Ed.)*, vol. 30, no. 4, pp. 355–360, Dec. 2013.

[25] L. Wu, H. Zha, C. Xiu, and Q. He, "Local path planning for intelligent vehicle obstacle avoidance based on dubins curve and tentacle algorithm," Guangzhou Automobile Group., Kunshan, China, Tech. Rep. 2017-01-1951, Sep. 2017.

[26] C. Chen, H. E. Yu-Qing, B. U. Chun-Guang, and J. D. Han, "Feasible trajectory generation for autonomous vehicles based on quartic Bézier curve," *Acta Automat. Sinica*, vol. 41, no. 3, pp. 486–496, Mar. 2015.

[27] X. Li, Z. Sun, D. Liu, Q. Zhu, and Z. Huang, "Combining local trajectory planning and tracking control for autonomous ground vehicles navigating along a reference path," presented at the IEEE Conf. Intell. Transp. Syst. (ITSC), Qingdao, China, Oct. 2014. [Online]. Available: https://ieeexplore.ieee.org/stamp/stamp.jsp?tp=&arnumber=6957775

[28] X.-X. Fu, Y.-H. Jiang, D.-X. Huang, J.-C. Wang, and K.-S. Huang, "Intelligent computing budget allocation for on-road trajectory planning based on candidate curves," *Frontiers Inf. Technol. Electron. Eng.*, vol. 17, no. 6, pp. 553–565, Jun. 2016.

[29] X. Fu, Y. Jiang, D. Huang, K. Huang, and J. Wang, "Trajectory planning for automated driving based on ordinal optimization," *Tsinghua Sci. Technol.*, vol. 22, no. 1, pp. 62–72, Feb. 2017.

[30] S. Yang and C. Li, "An enhanced routing method with Dijkstra algorithm and AHP analysis in GIS-based emergency plan," presented at the 18th Int. Conf. Geoinfor., Beijing, China, Jun. 2010. [Online]. Available: https://ieeexplore.ieee.org/stamp/stamp.jsp?tp=&arnumber=5567840

[31] R. M. de Lima, R. Osis, A. R. de Queiroz, and A. H. M. Santos, "Least-cost path analysis and multi-criteria assessment for routing electricity transmission lines," *IET Gener., Transmiss. Distrib.*, vol. 10, no. 16, pp. 4222–4230, Dec. 2016.
[32] M. Sahraei-Ardakani, M. Peydayesh, and A. Rahimi-Kian, "Multi attribute optimal DG planning under uncertainty using AHP method," presented at the IEEE Power Energy Soc. Gen. Meeting-Convers. Del. Elect. Energy 21st Century, Pittsburgh, PA, USA, Jul. 2008. [Online]. Available: https://ieeexplore.ieee.org/stamp/stamp.jsp?tp=&arnumber=4596815
[33] D. Q. Zhang, J.-F. Zhao, M.-H. Wang, and G.-H. Niu, "Grey evaluation and optimization of UAV's path planning method," presented at the 2nd Int. Conf. Electron. Comput. Technol., Kuala Lumpur, Malaysia, May 2010. [Online]. Available: https://ieeexplore.ieee.org/stamp/stamp.jsp?tp=&arnumber=5479981
[34] Z. Y. Gu and X. M. Li, "Research of state assessment for UAV based on FAHP," *Appl. Mech. Mater.*, vols. 599–601, pp. 2210–2214, Aug. 2014.
[35] X. Li, D. Zhou, Z. Yang, J. Huang, K. Zhang, and Q. Pan, "UAV route evaluation algorithm based on CSA-AHP and TOPSIS," presented at the IEEE Int. Conf. Inf. Automat., Macau, China, Jul. 2017. [Online]. Available: https://ieeexplore.ieee.org/stamp/stamp.jsp?tp=&arnumber=8079033
[36] X. Liu, W. Lin, Z. Lu, N. Jinhua, and Z. Xueyu, "AHP-based site planning of the logistics park," presented at the Int. Conf. Transp., Changchun, China, Dec. 2011. [Online]. Available: https://ieeexplore.ieee.org/stamp/stamp.jsp?tp=&arnumber=6199196
[37] A. K. Mishra, S. Deep, and A. Choudhary, "Identification of suitable sites for organic farming using AHP & GIS," *Egyptian J. Remote Sens. Space Sci.*, vol. 18, no. 2, pp. 181–193, Dec. 2015.
[38] K. R. Donevska, P. V. Gorsevski, M. Jovanovski, and I. Peševski, "Regional non-hazardous landfill site selection by integrating fuzzy logic, AHP and geographic information systems," *Environ. Earth Sci.*, vol. 67, no. 1, pp. 121–131, Sep. 2012.
[39] M. Elbanhawi, M. Simic, and R. N. Jazar, "Continuous path smoothing for car-like robots using B-spline curves," *J. Intell. Robot. Syst.*, vol. 80, no. 1, pp. 23–56, Dec. 2015.
[40] D. Q. Zeng, Z. Yu, L. Xiong, J. Zhao, P. Zhang, and Z. Fu, "A steerable curvature approach for efficient executable path planning for on-road autonomous vehicle," School Automot. Stud., Tongji Univ., Detroit, MI, USA, Tech. Rep. 2019-01-0675, Apr. 2019.
[41] D. Zeng, Z. Yu, L. Xiong, J. Zhao, P. Zhang, Z. Li, Z. Fu, J. Yao, and Y. Zhou, "A novel robust lane change trajectory planning method for autonomous vehicle," presented at the Intell. Vehicles Symp., Paris, France, Jun. 2019. [Online]. Available: https://ieeexplore.ieee.org/stamp/stamp.jsp?tp=&arnumber=8814151
[42] R. Zhang, L. Xiong, and Z. Yu, "Hierarchical control for reference trajectory tracking of autonomous vehicles," in *Proc. 25th Int. Symp. Dyn. Vehicles Roads Tracks*, Rockhampton, QLD, Australia, 2017, pp. 283–288.
[43] Z. Yu, R. Zhang, X. Lu, C. Jin, and K. Sun, "Robust adaptive anti-slip regulation controller for a distributed-drive electric vehicle considering the driver's intended driving torque," *Proc. Inst. Mech. Eng., D, J. Automobile Eng.*, vol. 232, no. 4, pp. 562–576, Aug. 2017.
[44] W. Timans, J. Antony, K. Ahaus, and R. van Solingen, "Implementation of lean six sigma in small- and medium-sized manufacturing enterprises in The Netherlands," *J. Oper. Res. Soc.*, vol. 63, no. 3, pp. 339–353, Mar. 2012.
[45] T. Baldassarre, N. Boffoli, D. Caivano, and G. Visaggio, "Managing software process improvement (SPI) through statistical process control (SPC)," in *Proc. Int. Conf. Product Focused Softw. Process Improvement*, Berlin, Germany, 2004, pp. 30–46.
[46] J. Antony, M. Kumar, and A. Labib, "Gearing six sigma into UK manufacturing SMEs: Results from a pilot study," *J. Oper. Res. Soc.*, vol. 59, no. 4, pp. 482–493, Apr. 2088.

DEQUAN ZENG received the master's degree from the School of Mechatronic Engineering and Automation, Shanghai University, Shanghai, China, in 2016. He is currently pursuing the Ph.D. degree with the School of Automotive Studies, Tongji University, Shanghai. His research interests include trajectory planning and decision making for autonomous vehicle.

ZHUOPING YU received the master's degree from Tongji University, Shanghai, China, in 1985, and the Ph.D. degree form Tsinghua University, Beijing, China, in 1996. He is currently a Professor and a Doctoral Supervisor with the School of Automotive Studies, Tongji University. His research interest includes vehicle engineering.

LU XIONG received the master's and Ph.D. degrees from Tongji University, Shanghai, China, in 2002 and 2005, respectively. He is currently a Professor and a Doctoral Supervisor with the School of Automotive Studies, Tongji University. His research interest includes vehicle engineering.

ZHIQIANG FU received the master's degree from Chinesisch-Deutsches Hochschulkolleg, Tongji University, Shanghai, China, in 2018, where he is currently pursuing the Ph.D. degree with the School of Automotive Studies. His research interests include motion controlling, trajectory planning, and decision making for autonomous vehicle.

PEIZHI ZHANG received the master's degree from the College of Automotive Engineering, Jilin University, Jilin, China, in 2014. He is currently pursuing the Ph.D. degree with the School of Automotive Studies, Tongji University, Shanghai, China. His research interests include trajectory planning, and simultaneous localization and mapping (SLAM) for autonomous vehicle.

HONGTU ZHOU is currently pursuing the master's degree with the College of Electronics and Information Engineering, Tongji University, Shanghai, China. His research interests include trajectory planning and decision making for autonomous vehicle.